Two new ene-reductases from photosynthetic extremophiles enlarge the panel of old yellow enzymes: *Ct*OYE and *Gs*OYE

Marina Simona Robescu[1] · Mattia Niero[1] · Mélanie Hall[2] · Laura Cendron[1] · Elisabetta Bergantino[1]

Abstract

Looking for new ene-reductases with uncovered features beneficial for biotechnological applications, by mining genomes of photosynthetic extremophile organisms, we identified two new Old Yellow Enzyme homologues: *Ct*OYE, deriving from the cyanobacterium *Chroococcidiopsis thermalis*, and *Gs*OYE, from the alga *Galdieria sulphuraria*. Both enzymes were produced and purified with very good yields and displayed catalytic activity on a broad substrate spectrum by reducing α,β-unsaturated ketones, aldehydes, maleimides and nitroalkenes with good to excellent stereoselectivity. Both enzymes prefer NADPH but demonstrate a good acceptance of NADH as cofactor. *Ct*OYE and *Gs*OYE represent robust biocatalysts showing high thermostability, a wide range of pH *optimum* and good co-solvent tolerance. High resolution X-ray crystal structures of both enzymes have been determined, revealing conserved features of the classical OYE subfamily as well as unique properties, such as a very long loop entering the active site or an additional C-terminal alpha helix in *Gs*OYE. Not surprisingly, the active site of *Ct*OYE and *Gs*OYE structures revealed high affinity toward anions caught from the mother liquor and trapped in the anion hole where electron-withdrawing groups such as carbonyl group are engaged. Ligands (para-hydroxybenzaldehyde and 2-methyl-cyclopenten-1-one) added on purpose to study complexes of *Gs*OYE were detected in the enzyme catalytic cavity, stacking on top of the FMN cofactor, and support the key role of conserved residues and FMN cofactor in the catalysis.

Keywords Biocatalysis · Ene-reductases · Extremophiles · OYE

Introduction

Ene-reductases (ERs) from the flavin mononucleotide (FMN)-containing old yellow enzyme (OYE) family of oxidoreductases (EC 1.6.99.1) constitute the main class of enzymes involved in C=C-double bond reduction reactions, performed at the expense of nicotinamide cofactors. These biocatalysts act on C=C-double bonds activated by at least one electron-withdrawing group (EWG); ideal substrates include α,β-unsaturated carbonyl and nitro compounds, and maleimides (Stuermer et al. 2007; Toogood et al. 2010). Based on sequence alignment, thus on typical fingerprint motifs (Oberdorfer et al. 2011; Litthauer et al. 2014), and quaternary structure, ERs have been historically clustered into two different classes: classical and thermophilic-like enzymes, with the latter generally considered more attractive for industrial applications due to their higher thermostability and wider pH and co-solvent tolerance. Few years ago, the increasing number of ERs being characterized inspired a phylogenetic analysis that distinguished three, instead of the two previously established, comprehensive groups: class I, containing many classical OYEs from plants, bacteria and cyanobacteria; class II, regarding exclusively classical enzymes from fungi; class III, grouping the traditional thermophilic-like OYEs. Such classification also seemed to better account for the differences in substrate preference among the diverse enzymes; a number of sequences, however, remained unassigned to any class (Scholtissek et al. 2017a). Indeed, the latter 'lost proteins' have been included in a very new and extended classification

✉ Laura Cendron
laura.cendron@unipd.it

✉ Elisabetta Bergantino
elisabetta.bergantino@unipd.it

[1] Department of Biology, University of Padova, Viale G. Colombo 3, 35131 Padova, Italy

[2] Department of Chemistry, University of Graz, Heinrichstrasse 28, 8010 Graz, Austria

that complements the previous one with two additional classes, which group proteins displaying sequence motifs associated with both classical and thermophilic OYEs (Peters et al. 2019).

The great majority of reported ene-reductases are derived from bacterial, fungal and plant sources, and generally operate under mild reaction conditions. A handful of ERs with improved thermostability has been isolated from extremophile organisms: TOYE, isolated from *Thermoanaerobacter pseudethanolicus* (Adalbjörnsson et al. 2010), chromate reductase CrS from *Thermus scotoductus* SA-01 (Opperman et al. 2010), *Gk*OYE from *Geobacillus kaustophilus* (Schittmayer et al. 2011) and FOYE from the acidophilic iron-oxidizing bacterium *Ferrovum* sp. JA12 (Scholtissek et al. 2017b).

The discovery of new ERs from extremophile organisms that show high stability along with excellent catalytic properties is of importance for biotechnological applications, as industrial processes often require robust catalysts able to operate under challenging conditions (such as high substrate concentration and temperature). Aiming at increasing the protein diversity of this class of enzymes, we initiated a search for OYE homologues in unconventional organisms such as photosynthetic extremophiles, by using as queries two sequences that are conventionally considered representative members for the classical and thermophilic-like subclasses. Among the putative enzymes identified, we selected two proteins: one from *Chroococcidiopsis thermalis*, a cyanobacterium, and a second one from *Galdieria sulphuraria*, an alga. To our knowledge, only higher plants (Magallanes-Noguera et al. 2017; Straßner et al. 2002; Straßner et al. 1999) and few examples of cyanobacteria (Fu et al. 2013; Fu et al. 2012) have been explored so far as source of ene-reductases so that simple, unicellular photosynthetic organisms represent an untapped reservoir of OYE homologues.

C. thermalis (*Ct*) is a coccoid cyanobacterium, adapted to live in extreme environments such as arid, hot and cold deserts. This organism generally lives on the surface of porous rocks or in biofilms at the stone-soil interface in desert pavements, resisting to dessication and freezing, as well as UVC and ionizing radiation (Friedmann et al. 1993; Warren-Rhodes et al. 2006; Fagliarone et al. 2017). Such peculiar and distinctive extreme tolerance is considered an adequate prerequisite to survival in the space, so that a species of this genus has been chosen as model for tests in space missions and ground-based Martian simulations (Billi et al. 2013).

G. sulphuraria (*Gs*) is a unicellular thermoacidophilic red alga able to grow in extreme conditions of pH (1.5–2.0) and temperature (> 56 °C) in volcanic hot springs. It also displays high salt and metal tolerance and exhibits an extraordinary metabolic versatility, being able to grow photoautotrophically, mixotrophically or heterotrophically on more than 50 carbon sources. The molecular foundations of such polyextremophilic phenotype have been investigated at the genomic (both nuclear and organellar) level and, interestingly, comparative genomics suggested the acquisition of protein families from extremophile bacteria or archaea through a previously unconceivable horizontal gene transfer mechanism (*i.e.* non-endosymbiosis related) (Schönknecht et al. 2013; Jain et al. 2014).

The two ene-reductases identified in these singular photosynthetic microbes (and named *Ct*OYE and *Gs*OYE), belonging to the subclass of classical ERs (along with the emblematic OYE1-3) (Stott et al. 1993; Niino et al. 1995), were produced in recombinant form and thoroughly characterized, up to the description of their crystal structures at 1.35 and 1.45 Å resolution, respectively. This study thus broadens the present landscape of ene-reductases, by adding two elements deriving from truly unconventional sources. It is worth underlining, in particular, that *Gs*OYE is the first classical ER discovered so far in a polyextremophile alga.

Materials and methods

Organisms and culture conditions

C. thermalis PCC 7203 was obtained from the Pasteur Culture Collection (Paris, France). Cells were grown photoautotrophically at 20 °C in BG11 medium. Static cultures were continuously illuminated at 25 mol photons $m^{-2} s^{-1}$. *G. sulphuraria* strain 074W was kindly provided by Dr. Antonino Pollio from the ACUF collection of the Biological Science Department of University Federico II, Naples, Italy. Cultures of *G. sulphuraria* were grown at 30 °C in Allen Medium pH 1.0 (Allen 1968) on a rotary platform shaker at 70 rpm. Light conditions used were 25 mol photons $m^{-2} s^{-1}$.

Sequence analysis and cloning

The NCBI database was used for DNA sequence analysis; searches and multiple alignments of *Ct*OYE and *Gs*OYE sequences were respectively produced by programs tBLASTn and Clustal Omega.

Genomic DNA of the cultured organisms was obtained following the DNA extraction method reported by Allen et al. (2006). Genomic DNA from *C. thermalis* or *G. sulphuraria* was used as template for an initial PCR amplification of a wider segment of DNA containing the coding sequence of interest; the obtained amplimers were then used with nested primers introducing the restriction sites *Nde*I and *Bam*HI at the 5′ and 3′ end of the open reading frames, respectively. The sequence of *Gs*OYE was also mutagenized in order to suppress an internal NdeI site. Sequence of the synthetic oligonucleotides used for PCR amplifications (CtOYE_1_for, CtOYE_2_rev, GsOYE_1_for, GsOYE_2_rev) and

mutagenesis (CtOYE_3_for, CtOYE_4_rev, GsOYE_3_for, GsOYE_4_rev, GsOYE_5_for, GsOYE_6_rev, GsOYE_7_for, GsOYE_8_rev) are reported in Table S1.

Expression vectors were produced by digestion of pET-28a(+) (Novagen, San Diego, CA) with *Nde*I/*Bam*HI (New England Biolabs, NEB) and ligation of the amplified *Ct*OYE and *Gs*OYE sequences, cut by the same enzymes.

Expression, analysis and purification of recombinant proteins

The recombinant enzymes were expressed in *E. coli* BL21 (DE3) (Novagen, San Diego, CA). Pre-cultures were carried out in 50 mL lysogeny broth medium (LB) containing 50 μg/mL kanamycin, at 37 °C. Preparative cultures were carried out in 1L LB; cells were grown in a shaking incubator (180 rpm) at 37 °C to an optical density at 600 nm (OD_{600}) of 0.4–0.6, then riboflavin (25 μM final concentration) and isopropyl-β-D-1-thiogalactopyranoside (IPTG, 0.2 mM final concentration) were added. After induction, cells were cultivated at 25 °C overnight. Cells were harvested by centrifugation (4 °C, 10 min, 5000×*g*) and washed with 50 mM Tris-HCl buffer pH 8.0. Cell disruption was obtained by French Press (Constant Systems Cell Disruptor OneShot; Constant Systems, Kennesaw, GA, USA) and crude extract was centrifuged (4 °C, 30 min, 18,000×*g*) to separate soluble and insoluble fractions. To enhance flavination, FMN cofactor (at 100 μM final concentration) was added to the crude extract before cell disruption. Expression of recombinant proteins was checked by SDS-PAGE analysis. The identity of the proteins was verified by immunoblotting using anti-His-tag antibodies. Overexpressed proteins were purified by immobilized-metal affinity chromatography (IMAC). Soluble fractions obtained from 1 L culture were incubated with 1 mL of Ni-NTA resin (Sigma Aldrich) for 30 min at 4 °C and then loaded and packed in a 10 mL empty Poly-prep® column (Bio-Rad). The column was washed by gravity flow with five column volumes of 50 mM Tris-HCl buffer pH 8.0. Elution was performed by five column volumes of 50 mM Tris-HCl pH 8.0 and 250 mM imidazole solution. Enzyme concentration was evaluated by spectrophotometric measurement of the concentration of free flavin in a solution of thermal denatured protein and calculated as previously reported (Fraaije et al. 2005).

For *Ct*OYE crystallization trials, an additional step for the removal of His$_6$-tag was performed following standard protocols (Sigma-Aldrich technical bulletin). Briefly, 10 mg of *Ct*OYE were digested using 50 μL of thrombin from human plasma (50 U) (Sigma Aldrich) overnight at 4 °C under mild shaking. A second IMAC chromatography purification was performed in order to remove His$_6$-tag and uncleaved protein.

A further purification step for the removal of thrombin was introduced using a prepacked Benzamidine Sepharose 4 Fast Flow column.

Analytical gel filtration

Size-exclusion chromatography assays were performed with an ÄKTA purifier system by using a Superdex 200 10/300 GL column (GE Healthcare) equilibrated with 50 mM Tris–HCl pH 8.0 and 150 mM NaCl. The flow rate for protein elution was 1 mL/min. β-Amylase (200 kDa), glucose oxidase (160 kDa), bovine serum albumin (66 kDa) and cytochrome c (12.4 kDa) were used as molecular mass standards. Apparent *M*r values of enzymes were obtained from a graph where the elution volume (Ve) of the standard proteins was plotted against log *M*w (Fig. S1).

Thermofluor measurements

Apparent unfolding temperatures of the recombinant enzymes, T_m, in standard conditions (50 mM Tris-HCl pH 8.0) and in the presence of different co-solvents (ethanol, acetone, acetonitrile, dimethylsulfoxide and dioxane) at different percentages (5–50% v/v), salts (NaCl, $(NH_4)_2SO_2$, $Na_3C_6H_5O_7$; 100–500 mM) and additives (glucose, glycerol, sorbitol, sucrose; 10–40% v/v) were determined using the Thermofluor method as described before (Fogal et al. 2015). Both *Ct*OYE and *Gs*OYE purified proteins were used, diluted to 5 μM in 50 mM Tris-HCl buffer pH 8.0. All measurements have been performed in triplicate.

Activity assay and kinetics

ER activity was determined by monitoring the consumption of NADPH at 340 nm (ε = 6.22 mM^{-1} cm^{-1}) using an Agilent 8453 spectrophotometer against a range of activated alkenes. In case of ketoisophorone (**7a**), the assay was performed at 365 nm using a molar absorption coefficient of 3.51 mM^{-1} cm^{-1} (Fu et al. 2013). The standard assay (100 μL) was performed at 25 °C in 50 mM Tris–HCl buffer pH 8.0 containing 10 μM NADPH and 10 mM substrate dissolved in 100% ethanol (1% final concentration). The reaction was started by adding the enzyme to 0.2 μM final concentration. One unit of ER activity is defined as the amount of protein that reduces 1 μmol NADPH per minute. Steady-state kinetic parameters of the different substrates were determined using substrate concentrations ranging from 0 to 25 mM. Data were fitted using the Michaelis–Menten equation by the program Graph-Pad Prism v5.0 (GraphPad Software, San Diego, CA, USA).

Determination of pH *optimum*

For the determination of the pH *optimum*, the specific activities (U/mg) were evaluated in a universal buffer of constant ionic strength (100 mM Tris, 50 mM MES and 50 mM AcOH) adjusted to the desired pH values (3–12) at 25 °C using either NaOH or HCl. The standard assay (100 μL) was performed using 100 μM NADPH and 10 mM 2-cyclohexen-1-one (**4a**) as standard substrate. Reactions were started by the addition of 0.2 μM purified enzyme and monitored over 1 min.

General procedure for enzymatic reduction reactions

Aliquots of enzymes to 100 μg/mL final concentration (~ 2.5 μM) were added to a Tris-HCl buffer solution (0.5 mL, 50 mM, pH 8.0) containing the substrate (10 mM) and the oxidised form of the cofactor (NAD$^+$, 100 μM), the cosubstrate (glucose, 20 mM) and the corresponding recycling enzyme (glucose dehydrogenase, 10 U/mL). For substrates **1a**, **2a**, **4a**, **5a**, **7a**, **8a** and **11a,** final substrate concentration of 50 mM was also tested. In this case, the following conditions were applied: 1 mM NAD$^+$, 100 mM glucose and 10 U/mL glucose dehydrogenase. Blank biotransformations without enzyme were performed as control reactions under same reaction conditions.

All substrates were added as a 1 M DMSO solution (1% final concentration) to overcome their poor solubility in water. The mixture was shaken at 30 °C and 140 rpm. After overnight incubation (that is from 16 to 18 h long), products were extracted with EtOAc (2 × 0.25 mL for 10 mM substrate and 4 × 0.25 mL for 50 mM substrate) containing 10 mM (*R*)-limonene as internal GC standard. The combined organic phases were dried over Na$_2$SO$_4$ and the resulting samples were analysed by GC.

For nitro compounds **15a**, **16a**, **17a** (10 mM), the reaction mixture was composed of Tris-HCl buffer solution (0.5 mL, 50 mM, pH 5.0–8.0), the oxidised form of the cofactor (NAD$^+$, 500 μM), the cosubstrate (glucose, 20 or 50 mM) and the corresponding recycling enzyme (glucose dehydrogenase, 10 U/ml). All substrates were added as a 1 M DMSO solution (1% final concentration). The mixture was shaken at different temperatures (10 °C, 25 °C and 30 °C) and 140 rpm. After overnight incubation, samples were processed as described above and analysed on GC-MS. All measurements have been performed in duplicate.

Analytical procedures employed for determining conversion and enantiomeric excess are described in detail in the Supplementary Materials.

Crystallization and data collection

Recombinant *Ct*OYE (20 mg/mL in 50 mM Tris-HCl buffer pH 8.0, 100 mM NaCl) and *Gs*OYE (20 mg/mL in 50 mM Tris-HCl buffer pH 8.0, 100 mM NaCl) were screened by high-throughput sparse matrix crystallization trials, dispensed by Oryx8 Robot (Douglas Instruments). MRC 96-well two-drop standard plates were adopted both in the initial screenings and following optimization steps. All the conditions were deposited and left equilibrating by vapour diffusion at 293 K. A panel of about 400 crystallization conditions were tested (JCSG, PACT, LMB and MORPHEUS screens, Molecular Dimension Ltd), combined with additive screens in the optimization steps. For further details, see Supplementary materials. X-ray diffraction data were collected at ESRF (Grenoble, France) synchrotron radiation source (for beamlines and data collections details, see Table S2).

Model building and refinement

All the diffraction data were processed and analysed by the automated pipelines feasible at ESRF synchrotron. In particular, we used the data integrated and scaled by EDNA Autoprocessing framework (XDS, XSCALE, Pointless, Aimless; Kabsch 2010). The obtained data were further cut to appropriate resolution by running aimless through the ccp4i2 suite (Winn et al. 2011). The same interface was used in combination with Phenix suite for any of the subsequent steps of phasing and refinement. *Ct*OYE data were processed in triclinic space group by EDNA Autoprocessing pipeline and further cut by Aimless to maximum resolution. Despite one of the cell angles being close to 90°, any attempts to process the data in higher symmetry space groups failed. The structure has been determined in the trigonal space group by Phaser software (McCoy et al. 2007) using as template the model of *Ct*OYE enzyme, built by Swiss model server (https://swissmodel.expasy.org). The refinement steps were carried out by Refmac5 (Skubak et al. 2004) and Phenix software Refine (Afonine et al. 2012). Flavin cofactor FMN was automatically imported from Coot dictionary and fitted by ligand search run. Final model includes four molecules per cell, 49% of solvent and final parameters Rfactor/Rfree of 0.22/0.25 and 1.35 Å resolution (further details can be found in Table S2). Protein structure was clear and well defined from residue Thr 3 to Glu 365, except for the fragment from Pro 269 to Glu 283, which was disordered and cannot be traced. FMN cofactor was easily placed and clearly defined in each of the four molecules present in the asymmetric unit. *Gs*OYE structure was determined by molecular replacement (MOLREP software, Vagin and Teplyakov 2010) using morphinone reductase (MR) from *Pseudomonas putida* as template (PDB: 1GWJ). After few cycles of refinement, the

most disordered regions and undefined loops were manually reconstructed with the support of Coot graphic interface (Emsley and Cowtan 2004). Structure refinement has been performed analogously to what was described for CtOYE. One molecule per asymmetric unit and roughly 46% of solvent define the crystal content. Final model was traced and fully visible from Met 1 to Arg 379, the last two amino acids being poorly defined in the density maps and thus omitted. Final parameters obtained for the best dataset (1.45 Å) reached Rfactor/Rfree of 0.18/0.19 (for further details see Table S2). Crystal structures of the complexes with substrates para-hydroxybenzaldehyde (pHBA) and 2-methyl-cyclopenten-1-one (MCP) were collected and processed analogously to GsOYE structure. Data were phased by molecular replacement using the GsOYE structure, previously determined, as template. Quite clear electron density not attributable to protein chain or FMN cofactor was observed in the difference maps and allowed to define the binding and orientation of pHBA and of MCP molecules in the active site of the respective complexes. Further traces of more pHBA molecules bound at the entrance of the catalytic cavity and in a peripheral region were detected. Geometry and restrains for any ligands were built and optimized by eLBOW (Moriarty et al. 2009). Details of data and models quality are reported in Table S2.

Results

Identification of the new putative ERs and sequence analysis

Two hypothetical proteins, the first one from the cyanobacterium C. thermalis (WP_015152687.1) and the second one from the polyextremophile red alga G. sulphuraria (XP_005703492), each annotated with an OYE-like FMN binding domain, were respectively identified by a tBLASTn search restricted to photosynthetic extremophile, using OYE1 from S. pastorianus (Q02899) as query sequence for classical ERs and YqjM from B. subtilis (P54550) as query for thermophilic-like enzymes. Search settings were initially restricted to red algae (taxid: 2763) or cyanobacteria (taxid: 117); then, in the obtained lists of sequences producing significant alignments, we manually search for putative sequences translated from extremophile genomes. The former prey protein, that we called CtOYE, showed 41% sequence identity with its bait OYE1. On the other hand, the thermophilic-like bait YqjM identified GsOYE, from G. sulphuraria, with which it shares 38% sequence identity. Despite this, both similarities observed in the sequence alignment (Fig. S2) and the results of the following biochemical analysis (see forward) showed that GsOYE has to be counted among classical ERs. In fact, beside the conserved catalytic pattern of all ERs that is H-xx-N/H-x-Y, it also displays the discriminating finger print motifs P-[LM]-T-R-x-R and G-[FYW]-xxx-P-G-[ILV]-[FHYW] (Oberdorfer et al. 2011). Sequence identity between CtOYE and GsOYE corresponds to 63%.

As expected on the bases of the limits imposed to the initial BLAST search, a phylogenetic analysis of the two putative enzymes together with 41 established ERs already present in the literature (and detailed in Fig. S3) indicates that CtOYE and GsOYE are more closely related to ERs identified in cyanobacteria (Fu et al. 2012; Fu et al. 2013) than to other ones from fungi or plants (Fig. S3). In particular, CtOYE shares high sequence identity (75% and 69%, respectively) with ERs isolated from the cyanobacteria Lyngbya sp. PCC8106 (LyngbyaER1) and Nostoc punctiforme (NospuncER1). GsOYE shows 60% and 51% sequence identity with Syn7048ER from Synecoccocus sp. PCC 7942 and CyanothER1 from Cyanothece sp. PCC 8801, respectively. As a further note, if the algal GsOYE is used as query sequence for an unrestricted tBLASTn search, no (putative) protein of eukaryotic origin is found among the first 100 results (which mostly include cyanobacterial proteins, in a range of identity from 64 to around 55%, and mostly proteobacterial proteins in the range down to 53%). Within Eukarya, the first homologue (50% identity) found in a photosynthetic organism is a putative 2-oxophytodienoate reductase 1 from the rice species O. brachyantha.

Purification of the recombinant proteins and evaluation of their thermal stability

CtOYE and GsOYE were expressed in the heterologous host E. coli BL21 (DE3) with an N-terminal His$_6$-tag. The recombinant proteins were mainly present in the soluble cell fraction and were purified by nickel affinity chromatography, displaying a yellow colour as expected for FMN binding polypeptides. Very high yields were obtained and could be further increased by optimizing the amount of resin used for IMAC chromatography (80 mg/L and 98 mg/L for CtOYE and GsOYE, respectively). Small amounts of proteins (negligible for GsOYE) were detected in the insoluble fractions, likely corresponding to unfolded species. For both CtOYE and GsOYE, impurities were almost completely eliminated after IMAC and SEC chromatography, as assessed by SDS-PAGE analysis; immunoblot-assays confirmed their identity as well as the purity of the preparations (Fig. 1a, b). The electrophoretic mobilities of the recombinant CtOYE and GsOYE were in line with the calculated molecular weights of 42.5 and 45.5 kDa, respectively. Moreover, analytical size-exclusion chromatography estimated molecular weights corresponding to those attended suggesting that both proteins occur as monomers in solution (Fig. 1c), analogously to OYEs belonging to the classical subclass.
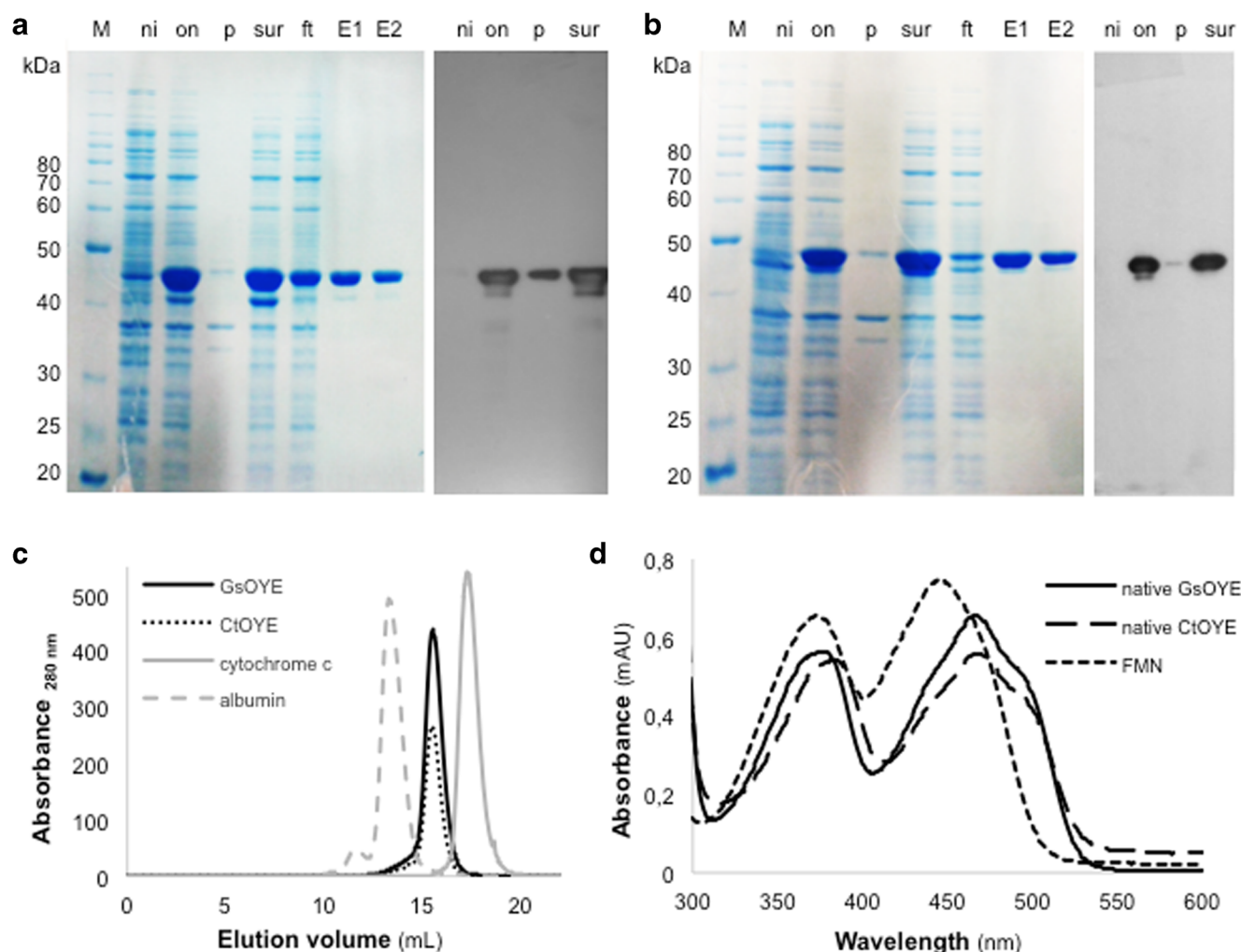
Fig. 1 Expression, purification and quantification of *Ct*OYE (**a**) and *Gs*OYE (**b**), 12% SDS-PAGE analysis of cell extracts from *E. coli* BL21 cells expressing the recombinant proteins: BenchMark™ protein ladder (M), total cell extracts from non-induced cells (ni) and overnight induced cells (on), pellet fraction (p), soluble protein fractions (sur), flow through (ft), pooled elution fractions from IMAC (E1) and from SEC (E2). Immunoblotting with anti-His-tag antibodies: non-induced cells (ni), overnight induced cells (on), pellet fraction (p), soluble protein fractions (sur). Analytical gel filtration (**c**) of purified *Ct*OYE (black dotted line) and *Gs*OYE (black continuous line) samples together with standard proteins cytochrome c (12.4 kDa) (grey continuous line) and serum albumin (66.5 kDa) (grey dashed line) eluted from a Superdex 200 10/300 GL column. Determination of *Ct*OYE and *Gs*OYE concentration (**d**) based on flavin content: UV–visible absorption spectra of purified enzymes and released flavin after thermal denaturation (dotted line)

The UV–visible absorbance spectra of purified *Ct*OYE and *Gs*OYE displayed maximum peaks at 468 nm and 465 nm respectively. In both cases, upon thermal denaturation, the supernatant turned into bright yellow and the maximum of its absorbance spectrum shifted to 446 nm (Fig. 1d), corresponding to the maximum of the released free FMN. These results suggested that the flavin prosthetic group of both ERs is non-covalently bound to the proteins.

Stability of both proteins was evaluated by detecting the apparent melting temperature (T*m*) using the Thermofluor method at different pH, in the presence of various salts, cryoprotectants and co-solvents. As reported in Table S3, the highest T*m* for *Gs*OYE was registered in aqueous buffer at pH 8.0 (67 °C ± 0.5 °C) while T*m* for *Ct*OYE (53 °C ± 0.5 °C) seemed constant over the tested pH range (6.5–8.0). NaCl was clearly preferred over ammonium sulphate, particularly by *Gs*OYE. Moreover, sorbitol appeared the best accepted cryoprotectant, leading to a maximal increase of 9 °C in the T*m* of *Ct*OYE and 7 °C in that of *Gs*OYE at 40% concentration. Therefore, once purified, the two proteins were generally conserved in 50 mM Tris-HCl pH 8.0, 150 mM NaCl and 40% sorbitol for following studies.

Finally, both enzymes exhibited good tolerance to the presence of up to 20 vol% DMSO, acetone and acetonitrile. A decrease in stability was detected with ethanol and dioxane, and a drop of up to 10 °C in T*m* was observed in 20 vol% dioxane with both proteins.

Steady-state kinetic parameters and cofactor preference

A preliminary spectrophotometric assay, based on the consumption of NADPH upon reduction of some α,β-unsaturated compounds, was performed in the initial stage of characterization of the two enzymes, and their specific activities are reported in Table S4. Steady-state kinetic parameters of CtOYE and GsOYE with the most promising substrates detected during the preliminary assay and kinetic parameters for the cofactors NAD(P)H were determined (Fig. 2 and Table 1). Highest substrate affinity (K_M of 6 μM with CtOYE and 17 μM with GsOYE) and activity ($k_{cat} = 12.42$ s^{-1} with CtOYE and 6.78 s^{-1} with GsOYE) were observed with maleimide (18a), resulting in catalytic efficiencies of 194 mM^{-1} s^{-1} for CtOYE and 399 mM^{-1} s^{-1} for GsOYE. 2-Cyclohexen-1-one (4a) was reduced with catalytic efficiencies of 3.53 and 2.68 mM^{-1} s^{-1} and K_M values of 1.0 and 2.1 mM for CtOYE and GsOYE, respectively. The introduction of the methyl group in α-position of 2-cyclohexen-1-one (5a) significantly reduced the activity of both enzymes toward the substrate, so that it was not possible to reach saturation levels and, thus, to determine the kinetic parameters for 5a (data not shown). The ring size had a significant effect on the kinetic parameters, as the catalytic efficiencies observed for both enzymes with 2-cyclopenten-1-one (1a) were very low (0.14–0.16 mM^{-1} s^{-1}). The aliphatic enal trans-2-hexen-1-al (20a) was a good substrate with catalytic efficiency of 9.08 mM^{-1} s^{-1} with CtOYE and 2.31 mM^{-1} s^{-1} with GsOYE.

Similar to most OYE homologues already described in literature (Toogood et al. 2010), CtOYE and GsOYE could accept both NADH and NADPH as cofactor with a slight preference for the latter one. The turnover frequency (k_{cat}) for NADPH was higher than that for NADH with both enzymes (46.71 s^{-1} for CtOYE and 11.41 s^{-1} for GsOYE). The apparent Michaelis constants (K_M) toward NADH and NADPH in the presence of maleimide for CtOYE were 0.43 mM and 0.053 mM, respectively (Table 1), while for GsOYE the constants were 0.38 mM and 0.054 mM, indicating higher binding affinity for NADPH than for NADH. Hence, NADPH appeared to be the preferred cofactor with catalytic efficiency (k_{cat} / K_M) twenty-seven-fold with CtOYE and nine-fold with GsOYE that of NADH.

The effect of pH on the reduction of 2-cyclohexen-1-one (4a) of both enzymes was investigated by monitoring the change in enzyme activity over a pH range 3.0–12.0 (Fig. S4). As a matter of fact, the activities remained high over wide pH ranges: CtOYE retained good activity between pH 5.0 to pH 8.0 with a slight amelioration (about 30%) at pH 9.0–10.0, while GsOYE retained 100% of activity from pH 5.0 to pH 9.0.

Fig. 2 α,β-Unsaturated compounds tested as substrates of CtOYE and GsOYE
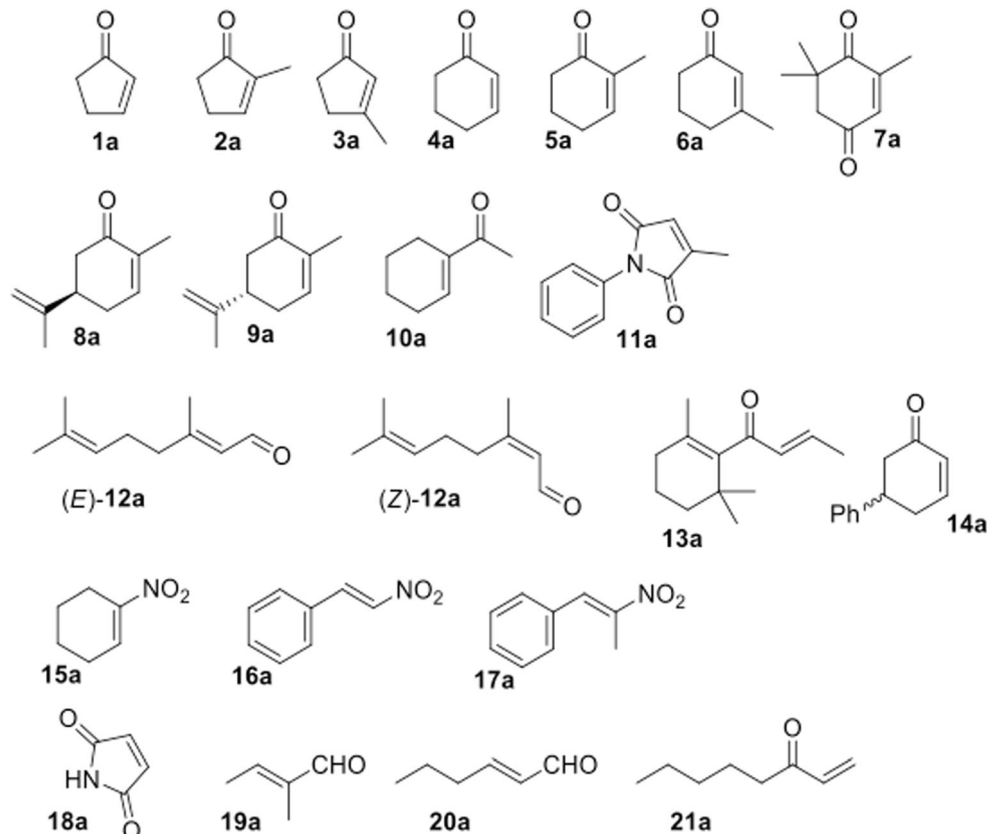
Table 1 Steady-state kinetic parameters of *Ct*OYE and *Gs*OYE[a]

Enzyme	Substrates	K_M (mM)	k_{cat} (s^{-1})	k_{cat}/K_M (mM^{-1} s^{-1})
*Ct*OYE	NADPH[b]	0.053 ± 0.009	46.71 ± 1.95	881.00
	NADH[b]	0.439 ± 0.031	14.27 ± 0.35	32.50
	Maleimide **18a**[c*]	0.006 ± 0.001	12.42 ± 0.28	1940.00
	2-Cyclopenten-1-one **1a**[c]	13.23 ± 2.47	2.09 ± 0.16	0.16
	2-Cyclohexen-1-one **4a**[c]	2.103 ± 0.489	5.65 ± 0.28	2.68
	Trans-2-hexen-1-al **20a**[c]	0.600 ± 0.038	5.43 ± 0.08	9.06
*Gs*OYE	NADPH[b]	0.054 ± 0.009	11.41 ± 0.52	203.00
	NADH[b]	0.388 ± 0.098	8.81 ± 0.71	22.70
	Maleimide **18a**[c]	0.017 ± 0.020	6.78 ± 0.17	399.00
	2-Cyclopenten-1-one **1a**[c]	15.54 ± 3.63	2.17 ± 0.17	0.14
	2-Cyclohexen-1-one **4a**[c]	1.079 ± 0.224	3.81 ± 0.23	3.53
	Trans-2-hexen-1-al **20a**[c]	1.908 ± 0.153	4.41 ± 0.10	2.31

[a] Standard assay (100–200 μL) was performed at 25 °C in 50 mM Tris-HCl (pH 8.0), 163 nM (* 16.3 nM) *Ct*OYE/ 180 nM *Gs*OYE and [b] 1 mM maleimide or [c] 100 μM NADPH. All measurements have been performed in triplicate

Bioreduction of activated alkenes

The substrate spectrum and stereoselectivity of *Ct*OYE and *Gs*OYE were investigated on a panel of α,β-unsaturated carbonyl compounds bearing various substitutions and representing typical substrates of the OYE family (**1a-14a**, Fig. 2). Overall, under standard conditions (10 mM substrate and GDH/glucose as NADH-recycling system), *Ct*OYE and *Gs*OYE displayed comparable behaviours in terms of activity and stereoselectivity (Table 2).

Non-substituted five-membered ring (**1a**) and six-membered ring (**4a**) were fully converted by both enzymes (Table 2). The influence of the substitution on activity and selectivity was striking. Moderate stereoselectivities were observed in the reduction of 2-methyl-cyclopenten-1-one (**2a**), which was converted into the (*S*)-enantiomer (70% *ee*) with low conversion levels (18% and 8% with *Ct*OYE and *Gs*OYE, respectively). Increasing the ring size from five (**2a**) to six carbon atoms (**5a**) led to a strong improvement in conversion (up to 88%) and stereoselectivity ((*S*)-**5b** > 99% *ee*). β-substituted analogues **3a** and **6a**, in contrast, were poorly converted, albeit with excellent stereoselectivity ((*S*)-**3b**/**6b** > 99% *ee*). Ketoisophorone (**7a**) and *N*-phenyl-2-methylmaleimide (**11a**), which are recognized as good substrates for OYEs, were quantitatively reduced (> 99% conversion) by both enzymes. With *Ct*OYE and *Gs*OYE, (*Z*)-**12a** was reduced to (*S*)-citronellal (**12b**) with higher stereoselectivity (up to 80% *ee* for (*S*)-**12b**) compared with the reduction of citral (mixture of (*E*)-**12a** and (*Z*)-**12a** 47:53, max. 37% *ee* for (*S*)-**12b**), indicating a possible influence of the alkene configuration on stereo-recognition. Finally, terpenoids (*R*)- and (*S*)-carvone (**8a** and **9a**) and 1-acetyl-1-cyclohexene (**10a**) were reduced with poor to moderate conversion

Table 2 Conversion of **1a**–**13a** (10 mM) in the reduction catalysed by ene-reductases *Ct*OYE and *Gs*OYE[a]

Substrate	*Ct*OYE		*Gs*OYE	
	Conv. (%)	ee (%)	Conv. (%)	ee (%)
1a	95	n.a.	97	n.a.
2a	18[#]	(*S*) 70	8	(*S*) 70
3a	ND (2[b])[d]	(*S*) > 99	2 (6[b])[d]	(*S*) > 99
4a	> 99	–	> 99	n.a.
5a	88	(*S*) > 99	88	(*S*) > 99
6a	1[#] (3[#b])[d]	(*S*) > 99	5 (9[#b])[d]	(*S*) > 99
7a	> 99	(*R*) 75	> 99	(*R*) 75
8a	2	(2*R*,5*S*) > 99	2	(2*R*,5*S*) > 99
9a	2	(2*R*,5*R*) > 99	2	(2*R*,5*R*) > 99
10a	18	n.a.	35	n.a.
11a	> 99	(*R*) > 99	> 99	(*R*) > 99
(*E*)/(*Z*)-**12a**[c]	9[d]	(*S*) 22	40[#d]	(*S*) 37
(*Z*)-**12a**[c]	9[#d]	(*S*) 55	48[#d]	(*S*) 80
13a	n.c.	n.a.	n.c.	n.a.

[a] The standard assay (500 μL) was performed at 30 °C and 120 rpm in 50 mM Tris-HCl (pH 8.0) containing 100 μM of NAD$^+$, 10 U/mL GDH, 20 mM of glucose and 10 mM of substrate. The reaction was started through the addition of enzyme to a final concentration of 100 μg/mL. All measurements have been performed in duplicate. The data points are mean values of duplicate reactions. Deviation from mean values was below 5% or below 10% where indicated ([#]). Conversion is based on product formation according to calibration curve; for **10a** and **11a**, it is based on substrate consumption according to calibration curve

[b] Standard conditions but with 300 μg/mL enzyme and incubated overnight

[c] The standard assay (500 μL) was performed at 30 °C and 120 rpm in 50 mM Tris-HCl (pH 8.0) containing 15 mM of NADH and 10 mM of substrate. The reaction was started through the addition of enzyme to a final concentration of 100 μg/mL and incubated for 6 h

[d] Conversion is apparent conv.% (area product/(area product + area substrate)*100). n.c. no conversion, n.a. not applicable

levels (max. 35% conversion). No conversion was observed with β-damascone (**13a**), most likely due to steric hindrance.

Further studies were performed aiming at increasing the initial substrate concentration (10 mM). In several cases (**1a**, **5a**, **7a** and **11a**), at 50 mM substrate concentration, conversions were limited to about 50% with both enzymes. In contrast, conversion level with **4a** was almost quantitative with *Gs*OYE, and a higher concentration was thus tested (100 mM). However, this appeared detrimental since conversion levels were reduced, likely due to inhibition or deactivation of both enzymes (Table S5).

A racemic mixture of 5-phenyl-2-cyclohexenone (**14a**) was used as starting material to test the ability of *Ct*OYE and *Gs*OYE to recognize a chiral centre distant from the reactive double bond, and thereby catalyse reductive kinetic resolution of *rac*-**14a** (Turrini et al. 2015) (Table 3). Both enzymes displayed good to moderate conversion levels (60% and 23% with *Ct*OYE and *Gs*OYE, respectively) and slight preference for the (*R*)-enantiomer in both cases.

*Ct*OYE and *Gs*OYE activity was next tested on a series of nitroalkenes (**15a-17a**, Fig. 2, Table 4). Overall, both enzymes allowed high conversion levels on these substrates, in line with the high reactivity of nitro-substituted alkenes (Toogood et al. 2008; Hall et al. 2007). Exception was the low conversion of **15a** by *Gs*OYE at pH 8 (25% conversion), which could be increased by lowering the pH to 5 (73% conversion). The pH had only minimal influence on activity level in the other cases. At pH 5.0, the bio-Nef pathway on nitro-compounds responsible for formation of oxime and carbonyl compound from **17a** (Durchschein et al. 2010) was more pronounced (up to 10% conversion to 1-phenyl-2-propanone **17c**). Despite various control reactions, it could not be clearly determined whether the biocatalytic equivalent of the Nef pathway was initiated

on **17a** or on **17b** (data not shown) (Toogood et al. 2011; Durchschein et al. 2010).
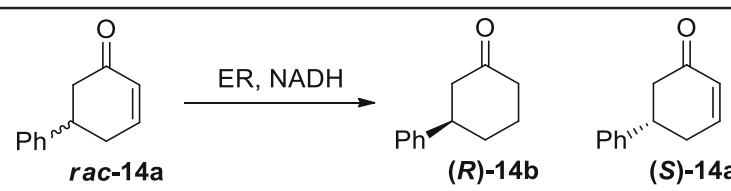
To prevent spontaneous racemisation of **17b** that occurs under aqueous conditions, reaction engineering was finally implemented by varying the reaction temperature and pH (Burda et al. 2013). At pH 5.0 and 10 °C, highest ee values were obtained: 70% and 50% (*R*)-**17b** from conversion with *Ct*OYE and *Gs*OYE, respectively (Table S6).

Crystal structures

The crystal structures of *Ct*OYE (PDB 6S32) and *Gs*OYE (PDB 6S0G) have been determined to high diffraction resolutions in both cases, 1.35 Å and 1.45 Å for *Ct*OYE and *Gs*OYE, respectively. Overall structures of *Ct*OYE and *Gs*OYE show the expected organization, following the highly conserved eight-stranded (α,β)-barrel fold of triosephosphate isomerase (TIM) and of all the other OYE family structures described till now (Fig. 3). Both accommodate FMN cofactor lying on top of the β-barrel core, at the C-terminus side, buried inside the active site cavity (for further details, see Supplementary Results). *Gs*OYE crystallized in the orthorhombic space group $P22_12_1$ with one molecule per asymmetric unit (ASU), while *Ct*OYE was solved and refined in P1 triclinic space group, with 4 molecules per ASU, not related by peculiar non crystallographic symmetries. While the overall fold, FMN binding site and fundamental residues in the catalysis are highly conserved, peculiar features have been disclosed for both enzymes. Indeed, main differences with other family members pertain the loops involved in substrate binding and cofactor preference, where amino acid residues critical for functional divergence are located.

Both three-dimensional structures are very similar to each other due to their high sequence identity and homology (64% sequence identity). *Ct*OYE and *Gs*OYE, analogously to very
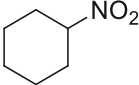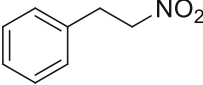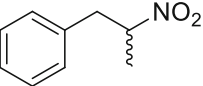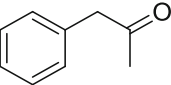
Table 3 Kinetic resolution of **14a**[a]

Enzyme	ee **14b** (%)	ee **14a** (%)	E	Conv. (%)[b]
*Ct*OYE	42 (*R*)	86 (*S*)	10	60
*Gs*OYE	72 (*R*)	22 (*S*)	8	23

[a] Reaction performed under standard conditions at 10 mM of substrate and 100 μg/L of enzyme; higher concentration of enzyme (up to 300 μg/mL) was also tested (data not shown) and led to no significant change in conversion levels. All measurements have been performed in duplicate. The data points are mean values of duplicate reactions. Deviation from mean values was below 5%

[b] Conversion calculated from [ee$_{substrate}$/(ee$_{substrate}$ + ee$_{product}$)]. Tool for calculation of E value (enantioselectivity) (Straathof and Jongejan 1997) available (open access) at http://biocatalysis.uni-graz.at/enantio/cgi-bin/enantio.pl

Table 4 Bioreduction of nitrocompounds **15a–17a** at various pH values[a]

Substrate	Main products	pH 8.0		pH 5.0	
		*Ct*OYE conv. (%)	*Gs*OYE conv. (%)	*Ct*OYE conv. (%)	*Gs*OYE conv. (%)
15a	NO$_2$ **15b**	99	25	97	73[#]
16a	NO$_2$ **16b**	89[#]	> 99	95	> 99
17a	NO$_2$ **17b**	> 95	> 99	n.t.	85[#]
	O **17c**	n.d.	1	n.t.	10

[a] The standard assay (500 μL) was performed at 30 °C and 120 rpm in 50 mM Tris-HCl (pH 8.0 and pH 5.0) containing 500 μM of NAD$^+$, 10 U/mL of GDH, 50 mM of glucose and 10 mM of substrate. The reaction was started through the addition of enzyme to a final concentration of 100 μg/mL and incubated overnight. The conversion reported is apparent conv. (area product/(area product + area substrate) *100). n.t. not tested; n.d. not detected. All measurements have been performed in duplicate. The data points are mean values of duplicate reactions. Deviation from mean values was below 5% or below 10% where indicated ([#])

few examples till now characterized in the OYEs family, have a very long loop 6, spanning from Glu 268 to Leu 297 for *Ct*OYE and from Glu 264 to Leu 279 for *Gs*OYE (for loop numbering see Fig. S2). In *Gs*OYE, this loop assumes an elongated and compact conformation, runs on enzyme surface, reaches the active site entrance, with residues from Gly 268 to Val 271 forming the β-hairpin turn directly contributing to size and features of the catalytic cavity (Fig. 3). *Gs*OYE Asn 270 points its side chain toward the top of the catalytic cavity (loop 3), opposite to FMN, and is stabilized in that orientation by a hydrogen bond with Tyr 346 of the C-terminal loop, closing the accession to the active site. The loop 6 of *Ct*OYE was highly flexible; its residues between Pro 269 and Leu 284 were disordered and could not be traced in the electron density map, as already reported for other OYE homologues (Breithaupt et al. 2001; Malone et al. 2005). Despite disordered, *Ct*OYE loop 6 composition is very similar to that of *Gs*OYE, with a conserved Asn 274 (Asn 270 in *Gs*OYE) as well as a clearly defined and superimposable Tyr 351 (Tyr 346 in *Gs*OYE). The cap subdomain region at the N-terminus, defined by the loop 3 on top of the active site entrance is indeed another hotspot in OYE enzymes family, since it has been demonstrated to interact with NADH/NADPH and tune the selectivity toward reducing cofactors (Pudney et al. 2007; Adalbjörnsson et al. 2010; Pompeu et al. 2012; Knaus et al.

2016). It shows high variability in terms of secondary structure content and size, ranging from α-helices to β-hairpins to largely unstructured turns, often occurring in parallel and in a compensatory manner with loop 6 variations. Indeed, in *Gs*OYE, while the loop 6 is long and extended till the FMN binding core, loop 3 shows a β-hairpin structure in an open conformation (Fig. 3). The loop 3 in *Ct*OYE is not organized in α-helices (as reported for OYE1) or β-sheets (as reported

Fig. 3 Cartoon representation of the crystal structures of *Ct*OYE (PDB: 6S32) (top left, slate purple) and *Gs*OYE (PDB: 6S0G) (top right, forest green) determined in this study. The most peculiar structural features of each enzyme are depicted in bright orange (loop 3, loop 6, and C-terminal helix in *Gs*OYE and loop 3 only in *Ct*OYE, given the flexible nature of loop 6 and absence of any C-term appendages). FMN cofactor bound in the active site is shown with C atoms in yellow; most relevant residues of the catalytic cavity are shown with orange C atoms, red O and blue N. In the bottom panels, from **a** to **d**, catalytic site details of the *Gs*OYE enzyme structures in complex with MCP (PDB: 6S23) (**a** and **c**) and pHBA ligands (PDB: 6S31) (**b** and **d**) are shown. In panels **a** and **b**, composite omit maps have been calculated and shown at 3.5 sigma (cyan). In panels **c** and **d**, details of the ligands binding mode and interactions established by pHBA and MCP and water molecules (W) eventually present in the close proximity to the ligands are evidenced. The two orientations of pHBA and MCP observed derived from alternative bindings observed either in the same active site (pHBA) or in the two molecules present in the asymmetric unit (MCP) are here superposed. The cavity surface is coloured according to electrostatic potential (qualitative calculation, Pymol 2.2.0 utilities)
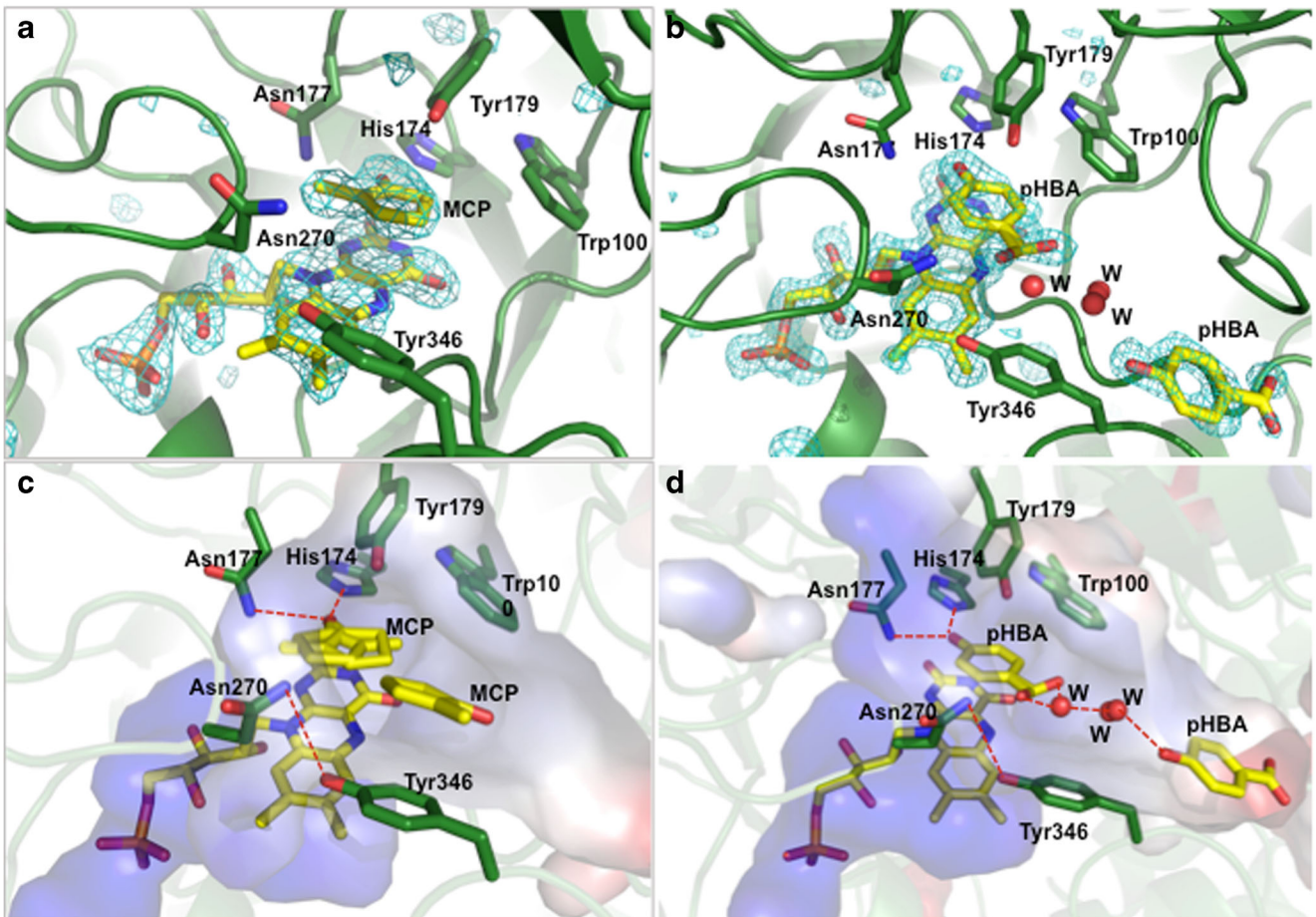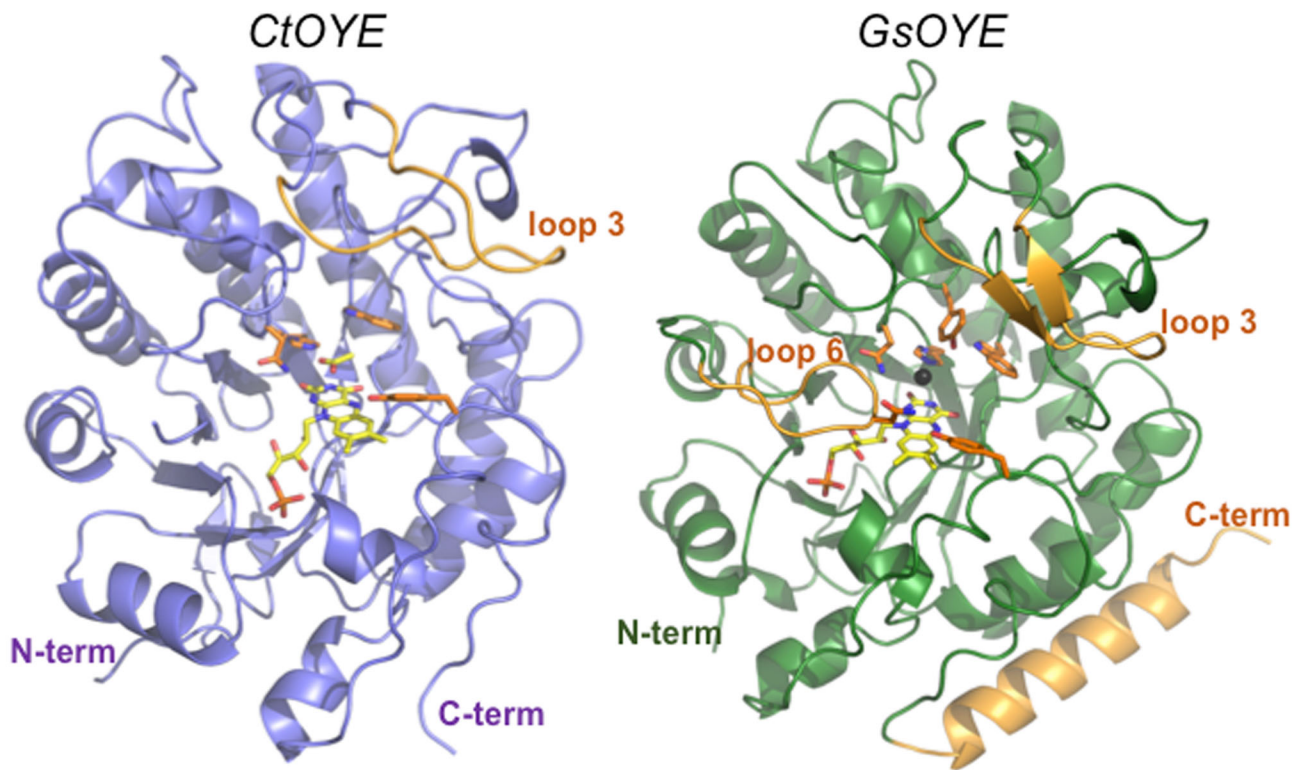
for *Gs*OYE, PETNR or SYE1) but it arranges into two largely unstructured turns (as described for OPR1, OPR3 and NerA). *Ct*OYE loop 3 is slightly shorter and it has an open orientation leaving the entrance of the active site more accessible to substrates and solvent (Fig. 3).

*Gs*OYE is further characterized by an extra unique C-terminal α-helix, about 19 amino acids long (from Asp 360 to Arg 379), never reported in this family. Such additional component contributes to the globular assembly of the enzyme, packing on one face of TIM barrel and establishing a large number of interactions with other two α-helices (Lys 37 to Ser 47 and Asp 75 to Arg 91).

All the key residues coordinating the FMN cofactor (see Supplementary Results for detailed description) and involved in the catalysis are highly conserved in *Ct*OYE and *Gs*OYE enzymes. As with other OYEs reported, *Ct*OYE and *Gs*OYE rely on His/Asn dyad for electron-withdrawing group coordination and Tyr lying on top of FMN for protonation of the substrate. The overall active site cavity of *Gs*OYE is quite deep and narrow and FMN heavily buried at the bottom of the catalytic tunnel.

In the active site of *Gs*OYE structure, a chloride anion, present in the crystallization solution, was found interacting with both His 174 and Asn 177 and positioned on the *si*-face of the isoalloxazine ring of FMN, as shown by the difference electron density map F_o-F_c (Fig. 3).

Analogously, *Ct*OYE trapped acetate anions, present in the precipitation solution, in the active site of all the protein molecules in the asymmetric unit. Acetate stacks on top of FMN isoalloxazine moiety and interacts through its carboxylic group with the catalytic residues His 178/Asn 181 and a water molecule close to Asn 181.

In the structures of the *Gs*OYE complexes, both para-hydroxybenzaldyde (pHBA; PDB: 6S31) (Fig. 3b, d) and 2-methyl-cyclopenten-1-one (MCP; PDB: 6S23) (Fig. 3a, c) lie on top of FMN, orienting their cyclic core parallel to the cofactor and favourable to establish π-stacking interactions. Both ones are further involved in hydrogen bonding with His 174/Asn 177 dyad through their hydroxyl and carbonyl groups, respectively.

The electron density maps of *Gs*OYE - pHBA complex (Fig. 3b) suggests that pHBA lies on top of FMN in two alternative orientations, that only differ by orientation of the aldehyde group, either pointing toward Asn 270 and Tyr 346 and forming hydrogen bonds with them or rotated by 180 degrees and pointing toward the active site entrance. In this second position, it is involved in a network of hydrogen bonds with water molecules and an additional molecule of pHBA bound in a peripheral site at the cavity mouth, between Pro 67 and Tyr 346. Different structures in complex with pHBA have been solved also for other OYE (such as OYE1 (1OYB), SYE1 (2GQ9), SYE4 (5K1K), OYE3 (5V4P) and NerA (4JIP)) and the interaction through the hydroxyl group with the His/Asn (His) dyad was reported for all

of them; to our knowledge, such double conformation was reported only in the case of *Tc*OYE (3ATZ) where the two orientations have been trapped in different chains present in the asymmetric unit (Okamoto et al. 2011). Analogous to pHBA, MCP substrate binds in two alternative conformations (Fig. 3c) in the two *Gs*OYE molecules present in the asymmetric unit. In both cases, MCP binds in the active site, parallel to FMN and trapped with the carbonyl group pointing toward His 174/Asn 177 catalytic binders. The two orientations are roughly coplanar, differing by a rotation of about 180° around the carbonyl group.

Discussion

While the number of available ene-reductases has grown significantly over the past decade (Winkler et al. 2018; Scholtissek et al. 2017a), the demand for new homologues displaying both high activity and tolerance to process conditions remains largely unmatched, mostly due to the limitations inherent to this class of enzymes such as poor substrate tolerance, modest turnover numbers, low stability under demanding industrial conditions and in some cases low stereoselectivities (Toogood and Scrutton 2018).

Looking for new enzymes, we have characterized two novel ene-reductases from extremophilic photosynthetic organisms, *Ct*OYE from *C. thermalis* and *Gs*OYE from *G. sulphuraria*. Identified by homology search, both proteins were successfully overexpressed in recombinant form and demonstrated to possess catalytic activity as ene-reductases. Indeed, *Ct*OYE and *Gs*OYE were highly active with the broadly accepted OYE substrate maleimide (**18a**) (17.5 and 7.1 U/mg, respectively), in line with reported activity for ERs isolated from cyanobacteria (0.90–29.58 U/mg) (Fu et al. 2013). They also displayed the highest activity on *trans*-2-hexen-1-al (**20a**) registered so far, to our knowledge, for ene-reductases isolated from photosynthetic organisms (4.4–6.9 U/mg, compared with 0.27–2.32 U/mg for cyanobacterial homologues, as reported in Fu et al. 2013). On the basis of the most recent classification criteria, both enzymes are assigned to class I OYEs (although *Gs*OYE had been recovered from genomic databases by the bait YqjM, which is a representative thermophilic-like member of class II, according to Peters et al. 2019). In agreement with the general behaviour of class I OYE enzymes, *Ct*OYE and *Gs*OYE size exclusion and crystals packing analysis exclude the presence of oligomers of physiological relevance. Also, the two loops 3 and 6 observed at the opposite sides of the catalytic cavities of the analysed crystals are characteristic of the overall structure of classical OYEs (see superposition of crystal structures in Fig. S5). These loops are critical for functional divergence among different enzymes, being involved in substrate binding and in determining accessibility. In particular, enrichment of acidic or basic residues throughout loop 3 are known to contribute in tuning the reducing cofactor selectivity of OYEs. Enzymes such as PETNR present basic residues in such region (PETNR Arg 130 or NerA Lys 127 or NemA His

135) and show a clear preference toward NADPH. *Ct*OYE and *Gs*OYE, with their more open and less pronounced acidic nature of loop 3, can accept both NADH and NADPH but prefer the latter one as reducing donor.

Both enzymes were well active in biotransformations performed on 10 mM substrate, with an overall preference for simple non-substituted cyclic enones (**1a** and **4a**). Ketoisophorone (**7a**) and *N*-phenyl-2-methylmaleimide (**11a**), which are typical ER substrates, were also converted to high extent. Both enzymes demonstrated similar stereoselectivity, which was high with most substrates tested, except with 2-methyl-cyclopenten-1-one (**2a**; MCP), a notoriously difficult substrate for most OYE homologues (Faber and Hall 2015). As observed in *Gs*OYE crystal structure, MCP binds in two orientations that are roughly coplanar, differing by a rotation of about 180° around the carbonyl group. Such rotation causes the symmetrical repositioning of double bond and methyl group, thus exposing opposite C=C-bond faces to hydride attack. As a consequence, the two alternative orientations could offer an explanation for the moderate stereoselectivity (70% *ee* (*S*)) in the reduction of MCP.

In contrast to the (*R*)-stereoselectivity of most OYEs reported in literature in the reduction of 2-cyclohexen-1-one (**5a**) to 2-methyl-cyclohexanone (**5b**), both *Ct*OYE and *Gs*OYE produced (*S*)-**5b** with exquisite selectivity. Only two other OYEs, KYE from *Kluyveromyces lactis* and *Yers*ER from *Yersinia bercovieri*, have shown similar stereopreference (Yanto et al. 2011). Surprisingly, both enzymes show only moderate sequence identity with these ene-reductases (38% identity shared with KYE and 50% identity with *Yers*ER). Noteworthy, (*S*)-selectivity on **5a** has been also observed with non-flavin enone reductase from plants (Hirata et al. 2000).

Both enzymes could tolerate concentrations up to 50 mM for almost all the substrates tested (leading to about 50% conversion), and up to 96% conversion was observed for **4a** with *Gs*OYE. Higher concentration of **4a** was however unfavourable under the tested reaction conditions, likely due to inhibition or deactivation of both enzymes (max. 34% conversion observed with *Ct*OYE).

In line with the presence of a strong electron-withdrawing group, nitro olefins **15a**-**17a** were excellent substrates for both proteins (up to > 99% conversion). With *Gs*OYE, however, a significant influence of the pH on the formation of **15b** was observed, which seems favoured at acidic pH, as well as on the extent of the alternate bio-Nef pathway (Durchschein et al. 2010), also higher at acidic pH. This unusual behaviour may be related to the origin of *Gs*OYE, isolated from a thermoacidophilic red alga. Further investigations will be required to delineate precisely what the contribution of the pH is in these two reactions.

The stereo-recognition of a distant δ-stereocenter in α,β-unsaturated compounds by *Ct*OYE and *Gs*OYE was also investigated. Both enzymes were found active in the reduction

of **14a** and displayed enantioselectivity (max. E value of 10) with (*R*)-enantiopreference, but with varying activity level. While moderate, this enantioselectivity allowed recovery of the non-converted (*S*)-5-methylcyclohex-2-enone in 86% *ee* with *Ct*OYE and access to (*R*)-3-phenylcyclohexanone in 72% *ee* with *Gs*OYE. So far, only a few OYE homologues (such as OYE3 and XenA) have displayed pronounced enantioselectivity (E value up to 49) in the reductive kinetic resolution of γ-substituted α,β-unsaturated lactone substrates (Turrini et al. 2015).

As previously mentioned, loops 3 and 6 are known determinants of peculiarities in substrate preferences and catalytic functionality of different OYEs, in virtue of their different amino acid compositions. Furthermore, loop 6 shows also large variability in terms of size and flexibility: from the very short one (7 aa long) of NemA (3GKA), that leaves the active site quite open and does not contribute to the catalytic properties of the enzyme, to the intermediate size loop 6 (12 aa) of MR (1GWJ), which partially protrudes toward the solvent and is still clearly defined, to the very long ones (12–18 aa) reported for SYE1 (2GQ9), OYE1 (1OYA) and OYE 2.6 (3TJL). The 15 aa-long loop 6 of *Gs*OYE presents Asn 270 residue in the turn position, close to FMN cofactor, which forms a hydrogen bond with Tyr 346 residue, so closing the exposure of the cofactor to the solvent. In MR OYE, C-terminal loop Tyr 356 has been demonstrated to play a role in both phenolic substrates and NADH binding, and loop 6 Trp 274 in SYE1 has been supposed to have a compensatory role, given its loss of hydroxyl group due to Tyr to Phe 350 replacement (Van Den Hemel et al. 2006; Pudney et al. 2007). By similarity, in *Gs*OYE both Asn 270 and Tyr 346 residues present the features necessary to trap the substrate and contribute to reductive half-reaction by hydrogen bonding interactions. Although similar in length and composition to that of *Gs*OYE, loop 6 of *Ct*OYE could not be traced into the crystals, suggesting higher structural flexibility and, possibly, better resilience of the enzyme to substrate accommodation.

Finally, even though both enzymes belong to the classical OYE subfamily, which mostly encompasses non thermo-resistant biocatalysts, they show a wide range of pH tolerance and solvent tolerance, comparable to that of thermophilic-like homologues. Reported melting points for classical OYEs range typically from 40 to 45 °C (*e.g.*, *Chr*-OYE1 T*m* = 40 °C (Pei et al. 2016) and XdpB T*m* = 39.8 °C (Zahradník et al. 2018)). Surprisingly, *Ct*OYE and *Gs*OYE (with T*m* of 53 °C and 67 °C, respectively) display significantly higher melting points (ΔT*m* = 15–25 °C), a property which renders these enzymes attractive for applications under demanding process conditions. While the source organisms typically grow in extreme environments, these two homologues are assigned to the subclass of classical OYE homologues and thus present atypical T*m* values, however, below that of most members of the subclass of thermophilic-like homologues (*e.g.*, TOYE T*m* > 70 °C (Adalbjörnsson et al. 2010),

GkOYE Tm = 76 °C (Schittmayer et al. 2011). Interestingly, this property is however not conserved throughout the subclass, and YqjM displays a melting point of 51 °C (Schittmayer et al. 2011), a value similar to that of wild-type XenA (50 °C) (Yanto et al. 2010).

In conclusion, we deliver two new enzymes, CtOYE and GsOYE, to the already rich panel of old yellow enzymes. The biocatalytic potential of the two enzymes for the asymmetric bioreduction of a wide spectrum of α,β-unsaturated ketones, aldehydes and nitro-alkenes has been duly described. Their thorough biochemical characterization, here presented, offers hints for understanding mechanistic details of the reduction of activated C=C-bonds and, possibly, suggestions for the rational engineering of their stereo-preference, still a limitation for the industrial use of this family of enzymes. The peculiar features of loop 6 and its direct impact on catalytic cavity features suggest that future mutagenesis studies targeting its size and composition could help tuning enzyme stereoselectivity and efficiency. Not least, the discovery of an OYE in a photosynthetic red alga (GsOYE), never described before, may represent a further phylogenetic clue for assessing/updating the current classification of these enzymes.

Compliance with ethical standards

This article does not contain any studies with human participants or animals performed by any of the authors.

Conflict of interest The authors declare that they have no conflict of interest.

References

Adalbjörnsson BV, Toogood HS, Fryszkowska A, Pudney CR, Jowitt TA, Leys D, Scrutton NS (2010) Biocatalysis with thermostable enzymes: structure and properties of a thermophilic ene-reductase related to old yellow enzyme. ChemBioChem 11:197–207. https://doi.org/10.1002/cbic.200900570

Afonine PV, Grosse-Kunstleve RW, Echols N, Headd JJ, Moriarty NW, Mustyakimov M, Terwilliger TC, Urzhumtsev A, Zwart PH, Adams PD (2012) Towards automated crystallographic structure refinement with phenix.Refine. Acta Cryst D 68:352–367. https://doi.org/10.1107/S0907444912001308

Allen MM (1968) Simple conditions for growth of unicellular blue-green algae on plates. J Phycol 4:1–4. https://doi.org/10.1111/j.1529-8817.1968.tb04667.x

Allen GC, Flores-Vergara MA, Krasynanski S, Kumar S, Thompson WF (2006) A modified protocol for rapid DNA isolation from plant tissues using cetyltrimethylammonium bromide. Nat Protoc 1(5):2320–2325. https://doi.org/10.1038/nprot.2006.384

Billi D, Baqué M, Smith HD, McKay CP (2013) Cyanobacteria from extreme deserts to space. Adv Microbiol 3:80–86. https://doi.org/10.4236/aim.2013.36A010

Breithaupt C, Strassner J, Breitinger U, Huber R, Macheroux P, Schaller A, Clausen T (2001) X-ray structure of 12-oxophytodienoate reductase 1 provides structural insight into substrate binding and specificity within the family of OYE. Structure 9:419–429. https://doi.org/10.1016/S0969-2126(01)00602-5

Burda E, Reß T, Winkler T, Giese C, Kostrov X, Huber T, Hummel W, Gröger H (2013) Highly enantioselective reduction of α-methylated nitroalkenes. Angew Chem Int Ed 52:9323–9326. https://doi.org/10.1002/anie.201301814

Durchschein K, Ferreira-Da Silva B, Wallner S, Macheroux P, Kroutil W, Glueck SM, Faber K (2010) The flavoprotein-catalyzed reduction of aliphatic nitro-compounds represents a biocatalytic equivalent to the Nef-reaction. Green Chem 12:616–619. https://doi.org/10.1039/b922691e

Emsley P, Cowtan K (2004) Coot: model-building tools for molecular graphics. Acta Cryst D 60:2126–2132. https://doi.org/10.1107/S0907444904019158

Faber K, Hall M (2015) Addition of hydrogen to C=C double bonds: alkene reduction. In: Faber K, Fessner WD, Turner NJ (eds) Science of synthesis: biocatalysis in organic synthesis. Georg Thieme Verlag, Stuttgart, pp 213–260

Fagliarone C, Mosca C, Ubaldi I, Verseux C, Baqué M, Wilmotte A, Billi D (2017) Avoidance of protein oxidation correlates with the desiccation and radiation resistance of hot and cold desert strains of the cyanobacterium *Chroococcidiopsis*. Extremophiles 21:981–991. https://doi.org/10.1007/s00792-017-0957-8

Fogal S, Beneventi E, Cendron L, Bergantino E (2015) Structural basis for double cofactor specificity in a new formate dehydrogenase from the acidibacterium *Granulicella mallensis* MP5ACTX8. Appl Microbiol Biotechnol 99:9541–9554. https://doi.org/10.1007/s00253-015-6695-x

Fraaije MW, Wu J, Heuts DPHM, van Hellemond EW, Spelberg JHL, Janssen DB (2005) Discovery of a thermostable Baeyer–Villiger monooxygenase by genome mining. Appl Microbiol Biotechnol 66:393–400. https://doi.org/10.1007/s00253-004-1749-5

Friedmann EI, Kappen L, Meyer MA, Nienow AJ (1993) Long-term productivity in the cryptoendolithic microbial community of the Ross Desert, Antarctica. Microb Ecol 25:51–69. https://doi.org/10.1007/BF00182129

Fu Y, Hoelsch K, Weuster-Botz D (2012) A novel ene-reductase from *Synechococcus* sp. PCC 7942 for the asymmetric reduction of alkenes. Process Biochem 47:1988–1997. https://doi.org/10.1016/j.procbio.2012.07.009

Fu Y, Castiglione K, Weuster-Botz D (2013) Comparative characterization of novel ene-reductases from cyanobacteria. Biotechnol Bioeng 110:1293–1301. https://doi.org/10.1002/bit.24817

Hall M, Stueckler C, Kroutil W, Macheroux P, Faber K (2007) Asymmetric bioreduction of activated alkenes using cloned 12-oxophytodienoate reductase isoenzymes OPR-1 and OPR-3 from *Lycopersicon esculentum* (tomato): a striking change of stereoselectivity. Angew Chem Int Ed 46:3934–3937. https://doi.org/10.1002/anie.200605168

Hirata T, Shimoda K, Gondai T (2000) Asymmetric hydrogenation of the C–C double bond of enones with the reductases from *Nicotiana tabacum*. Chem Lett 29:850–851. https://doi.org/10.1246/cl.2000.850

Jain K, Krause K, Grewe F, Nelson GF, Weber APM, Christensen AC, Mower JP (2014) Extreme features of the *Galdieria sulphuraria* organellar genomes: a consequence of polyextremophily? Genome Biol Evol 1:367–380. https://doi.org/10.1093/gbe/evu290

Kabsch W (2010) XDS. Acta Cryst D 66:125–132. https://doi.org/10.1107/S0907444909047337

Knaus T, Paul CE, Levy CW, De Vries S, Mutti FG, Hollmann F, Scrutton NS (2016) Better than nature: nicotinamide biomimetics that outperform natural coenzymes. J Am Chem Soc 138:1033–1039. https://doi.org/10.1021/jacs.5b12252

Litthauer S, Gargiulo S, Van Heerden E, Hollmann F, Opperman DJ (2014) Heterologous expression and characterization of the ene-reductases from *Deinococcus radiodurans* and *Ralstonia metallidurans*. J Mol Catal B 99:89–95. https://doi.org/10.1016/j.molcatb.2013.10.020

Magallanes-Noguera C, Cecati FM, Mascotti ML, Reta GF, Agostini E, Orden AA, Kurina-Sanz M (2017) Plant tissue cultures as sources of new ene- and ketoreductase activities. J Biotechnol 251:14–20. https://doi.org/10.1016/j.jbiotec.2017.03.023

Malone TE, Madson SE, Wrobel RL, Jeon WB, Rosenberg NS, Johnson KA, Bingman CA, Smith DW, Phillips GN Jr, Markley JL, Fox BG (2005) X-ray structure of *Arabidopsis* At2g06050, 12-oxophytodienoate reductase isoform 3. Proteins Struct Funct Genet 58:243–245. https://doi.org/10.1002/prot.20162

McCoy AJ, Grosse-Kunstleve RW, Adams PD, Winn MD, Storoni LC, Read RJ (2007) Phaser crystallographic software. J Appl Crystallogr 40:658–674. https://doi.org/10.1107/S0021889807021206

Moriarty NW, Grosse-Kunstleve RW, Adams PD (2009) Electronic ligand builder and optimization workbench (eLBOW): a tool for ligand coordinate and restraint generation. Acta Cryst D 65:1074–1080. https://doi.org/10.1107/S0907444909029436

Niino YS, Chakraborty S, Brown BJ, Massey V (1995) A new old yellow enzyme of *Saccharomyces cerevisiae*. J Biol Chem 270:1983–1991. https://doi.org/10.1074/jbc.270.5.1983

Oberdorfer G, Steinkellner G, Stueckler C, Faber K, Gruber K (2011) Stereopreferences of old yellow enzymes: structure correlations and sequence patterns in enoate reductases. ChemCatChem 3:1562–1566. https://doi.org/10.1002/cctc.201100141

Okamoto N, Yamaguchi K, Mizohata E, Tokuoka K, Uchiyama N, Sugiyama S, Matsumura H, Inaka K, Urade Y, Inoue T (2011) Structural insight into the stereoselective production of PGF2α by old yellow enzyme from *Trypanosoma cruzi*. J Biochem 150:563–568. https://doi.org/10.1093/jb/mvr096

Opperman DJ, Sewell BT, Litthauer D, Isupov MN, Littlechild JA, van Heerden E (2010) Crystal structure of a thermostable old yellow enzyme from *Thermus scotoductus* SA-01. Biochem Biophys Res Commun 393:426–431. https://doi.org/10.1016/j.bbrc.2010.02.011

Pei XQ, Xu MY, Wu ZL (2016) Two "classical" old yellow enzymes from *Chryseobacterium* sp. CA49: broad substrate specificity of *Chr*-OYE1 and limited activity of *Chr*-OYE2. J Mol Catal B 123:91–99. https://doi.org/10.1016/j.molcatb.2015.11.008

Peters C, Frasson D, Sievers M, Buller R (2019) Novel old yellow enzymes subclasses. ChemBioChem 20:1569–1577. https://doi.org/10.1002/cbic.201800770

Pompeu YA, Sullivan B, Walton AZ, Stewart JD (2012) Structural and catalytic characterization of *Pichia stipitis* OYE 2.6, a useful biocatalyst for asymmetric alkene reductions. Adv Synth Catal 354:1949–1960. https://doi.org/10.1002/adsc.201200213

Pudney CR, Hay S, Pang J, Costello C, Leys D, Sutcliffe MJ, Scrutton NS (2007) Mutagenesis of morphinone reductase induces multiple reactive configurations and identifies potential ambiguity in kinetic analysis of enzyme tunneling mechanisms. J Am Chem Soc 129:13949–13956. https://doi.org/10.1021/ja074463h

Schittmayer M, Glieder A, Uhl MK, Winkler A, Zach S, Schrittwieser JH, Kroutil W, Macheroux P, Gruber K, Kambourakis S, Rozzell JD, Winkler M (2011) Old yellow enzyme-catalyzed dehydrogenation of saturated ketones. Adv Synth Catal 353:268–274. https://doi.org/10.1002/adsc.201000862

Scholtissek A, Tischler D, Westphal AH, van Berkel WJH, Paul CE (2017a) Old yellow enzyme-catalysed asymmetric hydrogenation: linking family roots with improved catalysis. Catalysts 130:1–24. https://doi.org/10.3390/catal7050130

Scholtissek A, Ullrich SR, Mühling M, Schlömann M, Paul CE, Tischler D (2017b) A thermophilic-like ene-reductase originating from an acidophilic iron oxidizer. Appl Microbiol Biotechnol 101:609–619. https://doi.org/10.1007/s00253-016-7782-3

Schönknecht G, Chen WH, Ternes CM, Barbier GG, Shrestha RP, Stanke M, Bräutigam A, Baker BJ, Banfield JF, Garavito RM, Carr K, Wilkerson C, Rensing SA, Gagneul D, Dickenson NE, Oesterhelt C, Lercher MJ, Weber APM (2013) Gene transfer from bacteria and archaea facilitated evolution of an extremophilic eukaryote. Science 339:1207–1210. https://doi.org/10.1126/science.1231707

Skubak P, Murshudov GN, Pannu NS (2004) Direct incorporation of experimental phase information in model refinement. Acta Cryst D 60:2196–2201. https://doi.org/10.1107/S0907444904019079

Stott K, Saito K, Thiele DJ, Massey V (1993) Old yellow enzyme. The discovery of multiple isozymes and a family of related proteins. J Biol Chem 268:6097–6106

Straathof AJ, Jongejan JA (1997) The enantiomeric ratio: origin, determination and prediction. Enzym Microb Technol 21:559–571. https://doi.org/10.1016/S0141-0229(97)00066-5

Straßner J, Fürholz A, Macheroux P, Amrhein N, Schaller A (1999) A homolog of old yellow enzyme in tomato. Spectral properties and substrate specificity of the recombinant protein. J Biol Chem 274:35067–35073. https://doi.org/10.1074/jbc.274.49.35067

Straßner J, Schaller F, Frick UB, Howe GA, Weiler EW, Amrhein N, Macheroux P, Schaller A (2002) Characterization and cDNA-microarray expression analysis of 12-oxophytodienoate reductases reveals differential roles for octadecanoid biosynthesis in the local versus the systemic wound response. Plant J 32:585–601. https://doi.org/10.1046/j.1365-313X.2002.01449.x

Stuermer R, Hauer B, Hall M, Faber K (2007) Asymmetric bioreduction of activated C=C bonds using enoate reductases from the old yellow enzyme family. Curr Opin Chem Biol 11:203–213. https://doi.org/10.1016/j.cbpa.2007.02.025

Toogood HS, Scrutton NS (2018) Discovery, characterization, engineering, and applications of ene-reductases for industrial biocatalysis. ACS Catal 8:3532–3549. https://doi.org/10.1021/acscatal.8b00624

Toogood HS, Fryszkowska A, Hare V, Fisher K, Roujeinikova A, Leys D, Gardiner JM, Stephens GM, Scrutton NS (2008) Structure-based insight into the asymmetric bioreduction of the C=C double bond of α,β-unsaturated nitroalkenes by pentaerythritol tetranitrate reductase. Adv Synth Catal 350:2789–2803. https://doi.org/10.1002/adsc.200800561

Toogood HS, Gardiner JM, Scrutton NS (2010) Biocatalytic reductions and chemical versatility of the old yellow enzyme family of flavoprotein oxidoreductases. ChemCatChem 2:892–914. https://doi.org/10.1002/cctc.201000094

Toogood HS, Fryszkowska A, Hulley M, Sakuma M, Mansell D, Stephens GM, Gardiner JM, Scrutton NS (2011) A site-saturated mutagenesis study of pentaerythritol tetranitrate reductase reveals that residues 181 and 184 influence ligand binding, stereochemistry and reactivity. ChemBioChem 12:738–749. https://doi.org/10.1002/cbic.201000662

Turrini NG, Hall M, Faber K (2015) Enzymatic synthesis of optically active lactones via asymmetric bioreduction using ene-reductases from the old yellow enzyme family. Adv Synth Catal 357:1861–1871. https://doi.org/10.1002/adsc.201500094

Vagin A, Teplyakov A (2010) Molecular replacement with MOLREP. Acta Cryst D 66:22–25. https://doi.org/10.1107/S0907444909042589

Van Den Hemel D, Brigé A, Savvides SN, Van Beeumen J (2006) Ligand-induced conformational changes in the capping subdomain of a bacterial old yellow enzyme homologue and conserved sequence fingerprints provide new insights into substrate binding. J Biol Chem 281:28152–28161. https://doi.org/10.1074/M603946200

Warren-Rhodes KA, Rhodes KL, Pointing SB, Ewing SA, Lacap DC, Gómez-Silva B, Amundson R, Friedmann EI, McKay CP (2006) Hypolithic cyanobacteria, dry limit of photosynthesis, and microbial ecology in the hyperarid Atacama Desert. Microb Ecol 52:389. https://doi.org/10.1007/s00248-006-9055-7

Winkler CK, Faber K, Hall M (2018) Biocatalytic reduction of activated C=C-bonds and beyond: emerging trends. Curr Opin Chem Biol 43: 97–105. https://doi.org/10.1016/j.cbpa.2017.12.003

Winn MD, Ballard CC, Cowtan KD, Dodson EJ, Emsley P, Evans PR, Keegan RM, Krissinel EB, Leslie AGW, McCoy A, McNicholas SJ, Murshudov GN, Pannu NS, Potterton EA, Powell HR, Read RJ, Vagin A, Wilson KS (2011) Overview of the CCP4 suite and current developments. Acta Cryst D 67:235–242. https://doi.org/10.1107/S0907444910045749

Yanto Y, Hall M, Bommarius AS (2010) Nitroreductase from *Salmonella typhimurium*: characterization and catalytic activity. Org Biomol Chem 8:1826–1832. https://doi.org/10.1039/b926274a

Yanto Y, Winkler CK, Lohr S, Hall M, Faber K, Bommarius AS (2011) Asymmetric bioreduction of alkenes using ene-reductases *Yers*ER and KYE1 and effects of organic solvents. Org Lett 13:2540–2543. https://doi.org/10.1021/ol200394p

Zahradník J, Kolenko PP, Černý J, Kolářová L, Kyslíková E, Marešová H, Grulich M, Nunvar J, Šulc M, Kyslík P, Bohdan S (2018) The crystal structure of XdpB, the bacterial old yellow enzyme, in an FMN-free form. PLoS One 13:1–17. https://doi.org/10.1371/journal.pone.0195299

Supplementary Material to the Article

Two new ene-reductases from photosynthetic extremophiles enlarge the panel of Old Yellow Enzymes:

CtOYE and GsOYE.

Marina Simona Robescu[1], Mattia Niero[1], Mélanie Hall[2], Laura Cendron[1#], Elisabetta Bergantino[1#]

[1] Department of Biology, University of Padova, Viale G. Colombo 3, 35131 Padova, Italy

[2] Department of Chemistry, University of Graz, Heinrichstrasse 28, 8010 Graz, Austria

[#]**Corresponding authors email address**

Elisabetta Bergantino and Laura Cendron

elisabetta.bergantino@unipd.it (+39) 0498276342

laura.cendron@unipd.it   (+39) 0498276339

Table of Contents

Supplementary Materials and Methods

Analytical procedures for determination of conversion

GC–MS analyses were performed on a 7890A GC System (Agilent Technologies, Santa Clara, CA, USA), equipped with a 5975C mass selective detector. GC–FID analyses were carried out on a 7890A GC System (Agilent Technologies) equipped with an FID detector, and a 7683B Injector and a 7693 Autosampler by using H_2 or He as carrier gas (14.5 psi). HPLC analyses were performed by using a Shimadzu LC-20AD HPLC system equipped with a DGU-20 A5 degasser, a SIL-20AC autosampler, SPD-M20A diode array detector and a CTO-20AC column oven. Conversions of 2-cyclohexen-1-one (**4a**), 2-methyl-2-cyclohexen-1-one (**5a**) and 5-phenyl-2-cyclohexen-1-one (**14a**) were analysed by GC-FID using a 5% phenyl-dimethylpolysiloxane capillary column (HP-5 Agilent, 30 m, 0.32 mm, 0.25 μm), detector temperature 250 °C, split ratio 20:1. Programme for **4a**: 40 °C, hold for 2.0 min, 10 °C min-1 to 280 °C, hold for 1.0 min. Retention times were as follow: cyclohexanone (**4b**) 1.97 min, 2-cyclohexen-1-one (**4a**) 2.16 min. Programme for **5a**: 80 °C, hold for 10 min, 20 °C min-1 to 210 °C, hold for 2.0 min. Retention times were as follows: 2-methyl-cyclohexanone (**5b**) 6.07 min, 2-methyl-2-cyclohexen-1-one (**5a**) 6.89 min. Programme for **14a**: 80 °C, hold for 2 min, 10 °C min-1 to 280 °C, hold for 1.0 min. Retention times were as follow: 5-phenyl-cyclohexanone (**14b**) 10.8 min, 5-phenyl-2-cyclohexen-1-one (**14a**) 11.2 min.

Conversions of 2-cyclopenten-1-one (**1a**), 2-methyl-2-cyclopenten-1-one (**2a**), 3-methyl-2-cyclopenten-1-one (**3a**), 3-methyl-2-cyclohexen-1-one (**6a**), 1-acetylcyclohexene (**10a**), citral (**12a**) were determined using a 14% cyanopropylphenyl-dimethylpolysiloxane (DB-column 1701 Agilent, 30 m x 0.25 mm, 0.25 μm), detector temperature 250 °C, split ratio 20:1. Programme: 80 °C, hold for 10 min, 20 °C min-1 to 200 °C, hold for 2.0 min. Retention times were as follow: 2-cyclopentanone (**1b**) 3.59 min, 2-cyclopenten-1-one (**1a**) 4.74 min, 2-methyl-cyclopentanone (**2b**) 4.28 min, 2-methyl-2-cyclopenten-1-one (**2a**) 6.21 min, 3-methylcyclopentanone (**3b**) 4.57, 3-methyl-2-cyclopenten-1-one (**3a**) 10.5 min, 3-methylcyclohexanone (**6b**) 7.9 min, 3-methyl-2-cyclohexen-1-one (**6a**) 12.93 min, 1-acetylcyclohexane (**10b**) 11.2 min, 1-acetylcyclohexene (**10a**) 13.01 min, citronellal (**12b**) 13.51 min, neral and geranial (**12a**) 15.21 min and 15.56 min, respectively.

Conversions of ketoisophorone (**7a**), (*R*)-carvone (**8a**), (*S*)-carvone (**9a**), *N*-phenyl-2-methylmaleimide (**11a**) were determined using a 14% cyanopropylphenyl-dimethylpolysiloxane (DB-column 1701 Agilent, 30 m x 0.25 mm, 0.25 μm), detector temperature 250 °C, split ratio 20:1. Programme: 110 °C, hold for 5.0 min, 20 °C min-1 to 210 °C, hold for 6.0 min. Retention times were as follow: levodione (**7b**) 8.28 min, ketoisophorone (**7a**) 7.52 min, (*R*)-carvone (**8a**) and (*S*)-carvone (**9a**) 8.51 min, *trans*-dihydrocarvone (*trans*-**8b**) 7.85 min, *cis*-dihydrocarvone (*cis*-**8b**) 7.97 min, *N*-phenyl-2-methylsuccinimide (**11b**) 15.27 min, *N*-phenyl-2-methylmaleimide (**11a**) 13.36 min.

Conversions of β-damascone (**13a**) was analysed by GC-MS using a 5% phenyl-dimethylpolysiloxane capillary column (HP-5MS Agilent, 30 m x 0.25 mm, 0.25 μm), injector temperature 250 °C, split ratio 90:1. Programme: 100 °C, hold for 0.5 min, 10 °C min-1 to 300 °C. Retention times were as follow: **13a** 7.67 min.

For substrates **1a**-**10a**, calibration curves were obtained in the range 0-50 mM for both substrates and products using the internal standard. For substrate **11a**, a calibration curve was generated for the substrate only as the expected product was not available.

Conversions of 1-nitro-1-cyclohexene (**15a**), *trans*-β-nitrostyrene (**16a**), *trans*-β-methyl-β-nitrostyrene (**17a**), were analysed by GC-MS using a 5% phenyl-dimethylpolysiloxane capillary column (HP-5MS Agilent, 30 m x 0.25 mm, 0.25 μm), injector temperature 250 °C. Programme for **15a**: split ratio 20:1, 40 °C, hold for 2.0 min, 10 °C min-1 to 180 °C, hold for 1.0 min. Retention times were as follow: **15b** 10.35 min, **15a** 11.74 min. Programme for **16a** and **17a**: split ratio

90:1, 100 °C, hold for 0.5 min, 10 °C min-1 to 300 °C. Retention times were as follow: **16b** 6.28 min, **16a** 7.63 min, **17c** 4.35 min, **17b** 6.66 min, **17a** 8.15 min.

Analytical procedures for determination of enantiomeric excess and absolute configuration

Enantiomeric excesses of **2b**, **3b**, **6b** were determined using a 2,3-di-*O*-ethyl-6-*O*-*tert*-butyl dimethylsilyl β-cyclodextrin capillary column (Restek Rt-βDEXse, 30 m x 0.32 mm, 0.25 μm). Detector temperature 200 °C, injector temperature 180 °C, split ratio 25:1. Temperature programme for **2b**: 50 °C hold 5.0 min, 10 °C min-1 to 180 °C hold 1.0 min. Retention times were as follow: (*S*)-**2b** 11.28 min, (*R*)-**2b** 11.46 min, **2a** 12.64 min. Temperature programme for **3b**: 50 °C hold 2.0 min, 5 °C min-1 to 120 °C hold 2.0 min, 15 °C min-1 180 °C hold 2.0 min. Retention times were as follow: (*R*)-**3b** 12.53 min, (*S*)-**3b** 12.72 min, **3a** 17.01 min. Temperature programme for **6b**: 80 °C hold 10.0 min, 3 °C min-1 to 130 °C, 15 °C min-1 180 °C hold 2.0 min. Retention times were as follows: (*R*)-**6b** 18.07 min, (*S*)-**6b** 19.21 min, **6a** 28.0 min.

Enantiomeric excess of **5b** was determined using a 2,6-di-*O*-pentyl-3-trifluoroacetyl derivative of β-cyclodextrin capillary column (Chiraldex B-TA 40 m x 0.25 mm, 0.12 μm). Detector temperature 200 °C, injector temperature 180 °C, split ratio 25:1. Temperature programme for **5b**: 80 °C hold 2.0 min, 5 °C min-1 to 105 °C, 10 °C min-1 to 180 °C hold 4.0 min. Retention times were as follow: (*S*)-**5b** 7.4 min, (*R*)-**5b** 7.8 min.

Enantiomeric excess of **7b** was determined using a modified β-cyclodextrin capillary column (CP-Chirasil-DexCB 30 m x 0.25 mm, 0.25 μm). Detector temperature 200 °C, injector temperature 180 °C, split ratio 25:1. Temperature programme for **7b**: 90 °C hold 2.0 min, 4 °C min-1 to 115 °C, 15 °C min-1 to 180 °C hold 2.0 min. Retention times were as follow: (*R*)-**7b** 8.73 min, (*S*)-**7b** 8.95 min, **7a** 7.86 min.

Enantiomeric excess of **12b** was determined using a modified β-cyclodextrin capillary column (Hydrodex-β-TBDAc, 25 m x 0.25 mm). Detector temperature 200 °C, injector temperature 180 °C, split ratio 20:1. Temperature programme for **12b**: 60 °C hold 10.0 min, 1 °C min-1 to 105 °C, 15 °C min-1 to 180 °C, hold 3.0 min. Retention times: (*S*)-**12b** 52.13 min, (*R*)-**12b** 52.63 min, neral and geranial [(*Z*)- and (*E*)-**12a**)] 58.5 min and 59.4 min, respectively.

Enantiomeric excess of **11b** was determined on HPLC using a Chiralcel OD-H column (25 cm x 0.46 cm) and *n*-heptane/*i*-propanol 95:5 (isocratic) at 25 °C, flow 1 ml min-1. Retention times: (*R*)-**11b** 22.05 min, (*S*)-**11b** ND, **11a** 11.27 min.

Enantiomeric excess of **14b** was determined on HPLC using a Chiracel OJ column (25 cm x 0.46 cm) and *n*-heptane/*i*-propanol 99:1 (isocratic) at 25 °C, flow 0.5 ml min-1. Retention times: (*R*)-**14b** 14.74 min, (*S*)-**14b** 14.9 min, **14a** 13.59 min.

Enantiomeric excess of **17b** was determined on HPLC using a Chiralcel OJ column (25 cm x 0.46 cm) and *n*-heptane/*i*-propanol 90:10 (isocratic) at 25 °C, flow 0.8 ml min-1. Retention times: (*R*)-**17b** 13.22 min, (*S*)-**17b** 14.61 min, **17a** 10.0 min.

The absolute configuration of all products was determined based on comparison of elution profile with samples from reactions performed with homologues of known stereoselectivity or based on retention times from authentic reference samples.

Crystallization and data collection

Drops were prepared by mixing equal volumes (0.3 μL) of mother liquor and *Ct*OYE or *Gs*OYE (20 mg/mL in 50 mM Tris-HCl pH 8.0, 100 mM NaCl). Purified *Ct*OYE enzyme was reluctant to crystallize in the initial screenings. Few conditions gave very small irregular bunches of multiple crystals, unsuitable for crystallographic studies. To exclude the interference of His6-tag in the crystals nucleation and growth we proceeded with tag-cleavage by thrombin treatment as described before. The resulting recombinant enzyme was screened analogously to the previous ones and gave new

promising bunches of tiny crystals in multiple conditions. The best results were observed in LMB condition n.93 (0.85 M sodium citrate tribasic dihydrate, 0.1 M Tris pH 8.0, 0.1 M NaCl) which was used for crystals optimization by seeding techniques. Best crystals were obtained by using LMB condition n.93, micro-seeding from a seed stock prepared and stabilized in the same mother liquor and the addition of Fos-choline 12 additive (Rubic screen, Molecular Dimension Ltd), according to the following ratios (0.2 µL protein, 0.1 µL seeds stock, 0.2 µL precipitant agent supplemented with 0.15 mM Fos-Choline 12). On the other hand, initial clusters of small, irregular bunches of crystals of *N*-terminally His$_6$-tagged *Gs*OYE appeared after 5 days of incubation in multiple conditions (PACT screen n. 22 and 23, Structure screen n. 14, 32 and 42). Most regular ones (Structure screen n.22: 200 mM CaCl$_2$ dihydrate /100 mM MES, pH 6.0, containing 20 % w/v PEG 6000) where crashed and used to prepare a seeds stock used for crystals optimization by micro-seeding techniques: drops were prepared by mixing 0.2 µL of mother liquor, 0.1 µL seeds suspension and 0.3 µL of *Gs*OYE (20 mg/mL). Thicker and more regular crystals appeared in few days in PACT screen n. 22 and 23 (0.2 M MgCl$_2$ hexahydrate or 0.2 M CaCl$_2$ dihydrate, 0.1 M MES pH 6.0, 20 % w/v PEG 6000). Seeds stock and the above described crystallization conditions were used for any further crystallization trials with slight changes: for 2 µL drops size we added 1 µL mother liquor, 1 µL *Gs*OYE (20 mg/mL) and seeding with catfish. In this last setting, long rod-shaped single crystals appeared in 24 hours and rapidly grew to give high-resolution diffraction quality samples.

Crystals of *Gs*OYE in complex with known substrates were prepared by soaking apo-protein crystals with: para-hydroxybenzaldehyde (pHBA), 2-methyl-cyclopenten-1-one (MCP), and other substrates/inhibitors exploring a wide range of concentrations and different incubation times. In particular, a clear electron density describing the compounds complexing with *Gs*OYE were obtained for pHBA added in large excess by introducing few grains of powder directly into the drops and left diffusing for 30 minutes, while for MCP the best maps were obtained by incubating the crystals in a 10 mM solution of MCP. Finally, given the affinity of both inorganic and organic monovalent anions towards OYEs active site observed in multiple studies, we introduced a step of "crystals washing" with a 50% PEG 3350 solution before and/or in parallel to compounds soaking to remove such anions and allow the diffusion and binding of substrates of interest. Before freezing, the crystals were quickly soaked into a cryoprotectant solution composed of the precipitant agent supplemented with 20 % v/v ethylene glycol, and flash frozen in liquid nitrogen. X-ray diffraction data were collected at ESRF (Grenoble, France) synchrotron radiation source (for beamlines and data collections details see Table S2).

Supplementary Results

Description of FMN binding site and interactions

The key interactions involved into FMN coordination in *Ct*OYE are depicted in Fig. S6. Briefly, the N1 of flavin cofactor is in hydrogen contact with the side chain of Arg 230. The O2 atom is also interacting with the same residue Arg 230 but it establishes further interactions also with the side chain of Gln 101. This residue, Gln 101, is interacting as well as with the N3 of the flavin cofactor. The O4 of FMN is coordinated by a complex network of interactions with the backbone of Thr 28 and Ala 59. The N5 of the flavin is also in hydrogen contact with Thr28, that is supposed to modulate the FMN redox potential in classical OYEs. The dimethylbenzene moiety of the flavin isoalloxazine ring is stabilized by different hydrophobic interactions with residues Pro 26, Leu 27 and Tyr 351. The ribityl chain of the cofactor forms hydrogen bonds with Arg 230 and different hydrophobic interactions with Ala 25. The negative charged phosphate group of FMN is stabilized by the interaction with the positive charge of Arg 324 while the main chain atoms of Gly 302 and Gly 323 are involved in polar interactions with the phosphate group.

As shown in Fig. S6 the O4 of the flavin cofactor in *Gs*OYE is interacting with the backbone of Thr 25 and Ala 56. The N5 of the flavin is also in hydrogen contact with Thr 25, a highly conserved residue in classical OYEs known to be involved in the modulation of FMN redox potential. The N3 of the isoalloxazine ring is interacting with the side chain of Gln 98. The dimethylbenzene moiety of the flavin isoalloxazine ring is stabilized by different hydrophobic interactions with residues Leu 24, Asn 270 and Tyr 346. The ribityl chain of the cofactor forms one hydrogen bond with Arg 226 and different hydrophobic interactions with Gly 269 and Pro 23. The phosphate group of FMN which has a negative charge is stabilized by the positive charge of Arg 319 while the main chain atoms of Gly 297 and Gly 318 are involved in polar interactions with the phosphate group.

Supplementary Figures

Fig. S1. Calibration curve of Superdex 200 10/300 GL column (GE Healthcare) using standard proteins.

```
                                                      loop 1
                                          ◄──────────────────────►
OYE1    MSFVKDFKPGALGDTNLFKPIKIGNNFLLHRAVIPPLTRMRALHPGNIPNRDWAVEYYTQ    60
CtOYE   ----------MNTNIDLFSPVRLGRYELPNRMVMAPLTRNRAG-EGNVPR-ELNAEYYAQ    48
GsOYE   -------------MLKLLEPFDLNGLFLANRMVMAPLTRNRAG-PRFVPT-KMNALYYAQ    45
YqjM    -----------MARKLFTPITIKDMTLKNRIVMSPMCMYSSH-EKDGKLTPFHMAHYIS     47
                .*: *. :       * :* *: *:                :         :* .

                                      loop 2
                            ◄──────────────────────►
OYE1    RAQRPGTMIITEGAFISPQAGGYDNAPGVWSEEQMVEWTKIFNAIHEKKSFVWVQLWVLG    120
CtOYE   RVS--AGLIITEATQVSPQGLGYPFTPGIHSQEQVEGWRLVTKAVHDRGGKIFLQLWHVG    106
GsOYE   RSG--LGLIITEATQISQQGMGYPDTPGIYTDEQVDGWRMVTEAVHRREGCIFLQLWHVG    103
YqjM    RAIGGVGLIIVEASAVNPQGRITDQDLGIWSDEHIEGFAKLTEQVKEQGSKIGIQLAHAG    107
        *         :**.*.: :. *.       *: ::*::   :  : ::  : .: **    *

                                      loop 3
        ──────────────────────────────────────────────────────────►
OYE1    WAAFPDNLARDGLRYDSASDNVFMDAEQEAKAKKANNPQHSLTKDEIKQYIKEYVQAAKN    180
CtOYE   RISHPDLQVDGALPVAPSAIAPSEGMAATYEGEKPYVTPRALETAEIPGIVEQYRQGAKN    166
GsOYE   RVSHSSFQPNGQLPVAPSAIAPE-GEVMTYDGIKPFETPRALETEEVAHIVEDYRKAAIN    162
YqjM    RKAELEG-----DIFAPSAIAFD---------EQSATPVEMSAEKVKETVQEFKQAAAR     152
        :  .         ::           :           :       ::   :::: :.* .

                                      loop 4
                          ◄──────────────────────►
OYE1    SIAAGADGVEIHSANGYLLNQFLDPHSNIRTDEYGGSIENRARFTLEVVDALVEAIGHEK    240
CtOYE   AILAAGFDGVEIHSANGYLLDQFLHDGSNHRTDEYGGSIENRARLLMEVTEAVVSVWGADR   226
GsOYE   AKRAGFDGIEIHSANGYLLHEFLEDGTNKRTDRYGGSIENRARIVFEVLDAVCKVYPSRR    222
YqjM    AKEAGFDMIEIHAAHGYLIHEFLSPLSNHRTDEYGGSPENRYRFLREIIDEVKQVWDGPL    212
        :   ** *  :***:*:***..:**   :* ***.**** *** *:   *: : :  ..

                       loop 5                                loop 6
              ◄──────────────────►                 ◄──────────────
OYE1    VGLRLSPYGVFNS-MSGGAETGIVAQYAYVAGELEKRAKAGKRLAFVHLVEPRVTNPFLT    299
CtOYE   VGVRLSPSGTFGS-VYDSD---LKALFTYVVDALNQ-----FELAYLHLVEPRVAGNETV    277
GsOYE   VGIRLSPDTEFMS-MSDSD---RPALYSYLVQELSR-----RELAYLHLIEPRIKGNVDV    273
YqjM    F-VRVSASDYTDKGLDIADHIGFA---KWM-KE------QG-----VDLIDCS-SGALVH    255
        .  :*:*      . :   .          ::               :.*::    .

        ──────────────────►       loop 7              loop 8
                                ◄────────►        ◄──────────────
OYE1    EGEGEYEGGSNDFVYSIWKGPVIRAGNFA---LHPEVVREEVKDKRTLIGYGRFFISNPD    356
CtOYE   ENP--TSELSSKYFRPIYKGTLISAGGYD---RESGNAVL-ASGDADLVAYGRLFISNPD    331
GsOYE   EKE---SSLNVEFFRPLYKGVLITAGGYQ---KETGEERL-QKQHADLVAYGRWVIANPD    326
YqjM    ADINVFPGYQVSFAEKIREQADMATGAVGMITDGSMAEEILQNGRADLIFIGRELLRDPF    315
        . .:       : :  : :*         .         *:   **   .: :*

        ──────────►
OYE1    LVDRLEKGLPLNKYDRITFYQMSAHGYIDYPTYEEALKL----------GWDKK    400
CtOYE   LPQRFALNAQLNPYDRSSFYGGDKRGYTDYPSLELQAAG-------------    370
GsOYE   LPSRFEQNAPLNPYDRATFYGGNEKGYTDYPFLDPRDSQEALKEAEAAFRKWRRL    381
YqjM    FARTAAKQLNTE------------------------IPAPVQYERGW---    338
        :           :
```

Fig. S2 Sequence alignment of the two putative ERs from *Chroococcidiopsis thermalis* and *Galdieria sulphuraria*, performed by Clustal Omega. The catalytic residues are highlighted in purple and the finger print motifs reported by Oberdorfer et al. (2011) are highlighted in pink and yellow for classical ERs and green and cyan for thermophilic-like ERs. The boxes shaded in grey show the conserved residues, and the unshaded boxes indicate similar residues. Boxes highlighted in orange show the sequence conservation of FMN binding.

Fig. S3. Phylogenetic relationship of amino acid sequences of *Ct*OYE and *Gs*OYE to other 41 known OYEs

Gox 2684 (GI: 58038436) and Gox 0502 (GI: 58038972) from *G. oxydans*, NCR from *Z. mobilis* (GI: 409107016), OYE1 (Q02899.3) from *S. pastorianus*, OYE2 (Q03558.3) and OYE3 (P41816.2) from *S. cerevisiae*, OPR1 (CAB43506.1) and OPR3 (NP_001233873.1) from *S. lycopersicum*, Foye-1 (WP_056929840) from *Ferrovum* sp., *Dr*ER from *D. radiodurans* (NP_295913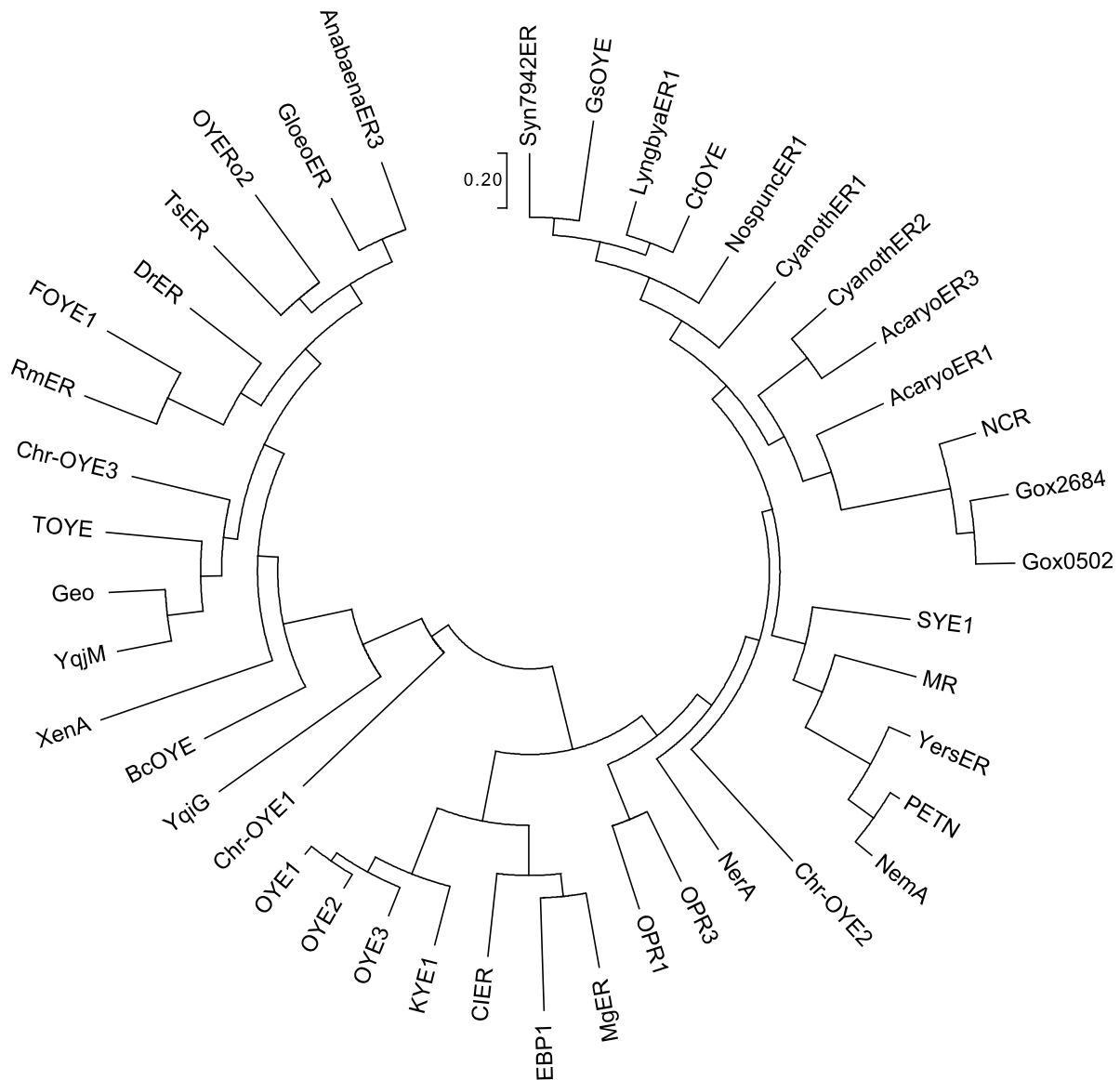.1), XenA from *P. putida* (P54550.3), *Rm*ER from *C. metallidurans* (WP_011519282.1), OYERo2 from *R. opacus* 1CP (ALL54975), *Ts*ER from *T. scotoductus* (CAP16804.1), TOYE from *T. pseudethanolicus* (ABY93685), YqjM from *B. subtilis* (BAA12619), Chr-OYE1 (ALE60336.1), Chr-OYE2 (ALE60337.1) and Chr-OYE3 (AHV90721.1) from *Chryseobacterium* sp. CA49, Geo from *Geobacillus* sp. no. 30 (BAO37313), KYE1 from *K. lactis* (P40952.2), NerA from *A. tumefaciens* (CAA74280), EBP1 from *C. albicans* (AAA18013.1), MR from *P. putida* (AAC43569.1), NemA from *E. coli* (BAA13186), PETNR from *E. cloacae* (AAB38683.1), Syn7942ER from *Synechococcus* sp. PCC 7942 (YP 399492), *Bc*OYE (AHN92003.1) from *B. coagulans*, GloeoER (NP_926774.1) from *G. violaceus* PCC 7421, YersER (WP_032896199.1) from *Y. bercovieri*, SYE1 from *S. oneidensis* (AAN55488.1), LyngbyaER1 (ZP_01620253.1) from *Lyngbya* sp. PCC 8106, AnabaenaER3 (WP_011316754.1) from *A. variabilis* ATCC 29413, *Mg*ER (XP_001482000.1) from *M. guilliermondii* ATCC 6260, CyanothER1 (WP_012593487.1) and CyanothER2 (WP_012594996.1) from *Cyanothece* sp. PCC 8801, AcharyoER1 (WP_012165090.1) and AcharyoER3 (WP_012167636.1) from *A. marina* MBIC11017, NospuncER1 (WP_012412475.1) from *N. punctiforme* PCC 73102, YqiG (NP_390301.1) from *B. subtilis* str.168, CIER (XP_002615481.1) from *C. lusitaniae* ATCC 42720.
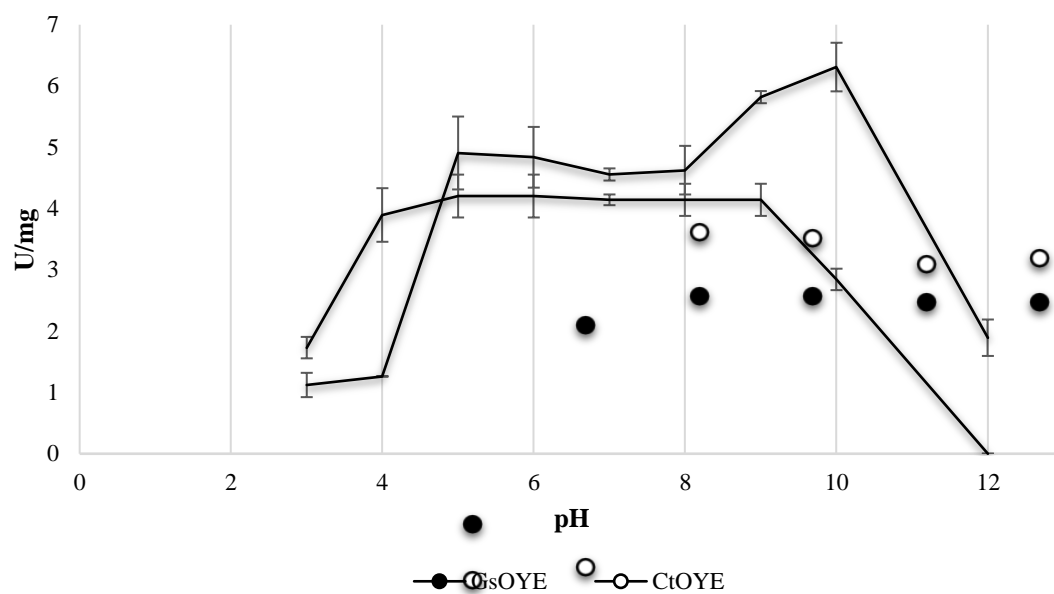
Fig. S4. *Ct*OYE (white circles) and *Gs*OYE (black circles) activity-pH profile.

The specific activity (U/mg) was determined by monitoring the reduction of 2-cyclohexen-1-one in the presence of NADPH. A universal buffer of constant ionic strength: 100 mM Tris-HCl, 50 mM MES, and 50 mM AcOH adjusted to the following pH values at 25 °C using 5 M NaOH or 5 M HCl: 3.0, 4.0, 5.0, 6.0, 7.0, 8.0, 9.0, 10.0, 11.0 and 12.0, was used to determine the activity of both enzymes.
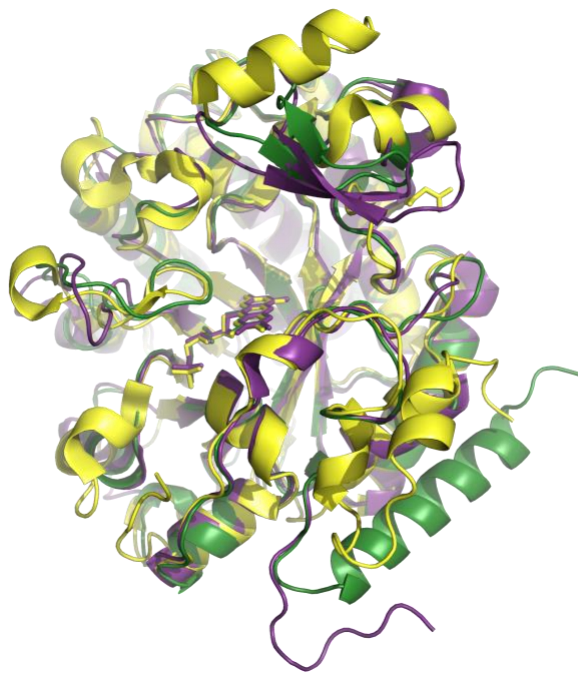
Fig. S5 Superposition of the crystal structure of *Gs*OYE with representative members of classical OYE family, (OYE 2.6 from the Xylose-fermenting fungus *Pichia stipites*, PDB: 3TJL, in yellow, and morphinone reductase (MR) from *Pseudomonas putida*, used as template in the molecular replacement, in purple PDB: 1GWJ).
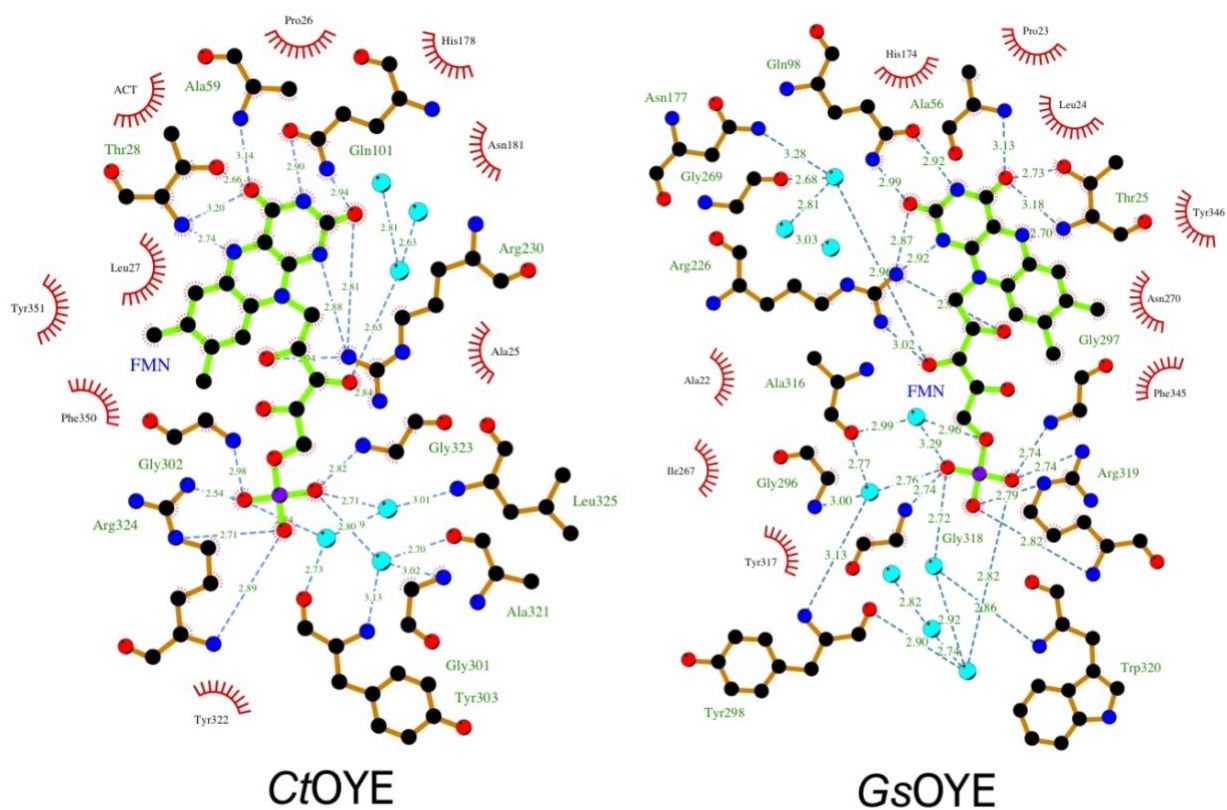
Fig. S6. Plot of FMN cofactor interactions in the active site of holo enzymes *Ct*OYE and *Gs*OYE. The interactions have been calculated and visualized by LigPlus software. The thin green dotted lines illustrate hydrogen bonds.

Supplementary Tables

Table S1. Oligonucleotides used for PCR amplification of *Ct*OYE and *Gs*OYE sequences and cloning. Restriction sites are shown in bold. Modifications introduced to mutate the original sequences are underlined.

| Primer	sequence (5'→3')	purpose
CtOYE_1_for	CAATTTTCAATCTGGTGGGGTCGGC	
CtOYE_2_rev	ACAGTTGCGATCGAGTAGGATTCGC	
CtOYE_3_for	CATTTACCCTAGTAAAG**CATATG**AATACCAACATCG	*Nde*I site introduction
CtOYE_4_rev	ATTA**GGATCC**TCAACCAGCAGCCTGCAATTCCAAAG	*Bam*HI site introduction
GsOYE_1_for	CGTCCGTTGTAGTTAGTGGACGGT	
GsOYE_2_rev	TGCGAGTCATCCAACAGAACAACT	
GsOYE_3_for	TGGACGGTGA**CATATG**TTGAAGC	*Nde*I site introduction
GsOYE_4_rev	ATAGTTTT**GGATCC**TTTGTGGAAGAC	*Bam*HI site introduction
GsOYE_5_for	GACCTCGTAGCGTATGGTCGTTG	*Nde*I site suppression
GsOYE_6_rev	CAACGACCATACGCTACGAGGTC	*Nde*I site suppression
GsOYE_7_for	CCATTGAAAATAGGGCGAGAATTGTG	Putative glycosylation site suppression (T204A)
GsOYE_8_rev	CACAATTCTCGCCCTATTTTCAATGG	Putative glycosylation site suppression (T204A)

Table S2. X-ray crystallographic data collection and refinement statistics for *Ct*OYE and *Gs*OYE (pHBA: p-hydroxybenzaldehyde; MCP: 2-methyl-cyclopenten-1-one)

	*Ct*OYE	*Gs*OYE	*Gs*OYE-pHBA	*Gs*OYE-MCP
Data collection statistics				
PDB code	6S32	6S0G	6S31	6S23
Wavelenght	1.00	1.0725	0.966	0.966
Space group	P1	P2 21 21	P2 21 21	P1 21 1
Cell constants				
a, b, c (Å)	49.65 78.17 108.68	56.75 76.66 88.60	57.05 76.29 88.12	56.69 76.42 86.33
α, β, γ (°)	104 100 90	90 90 90	90 90 90	90 93 90
Resolution range for refinement (Å)	48.86 – 1.35 (1.39 – 1.35)	45.61 – 1.45 (1.48 – 1.45)	57.05 – 1.63 (1.69 – 1.63)	57.18 – 2.4 (2.47 – 2.38)
Total reflections	1111221 (105276)	880814 (45283)	300625 (12407)	94042 (10017)
Number of Unique Reflections	312849 (29361)	69197 (3504)	48778 (4758)	29511 (3122)
R_{merge}	0.086 (0.535)	0.07 (0.63)	0.21 (0.46)	0.093 (0.113)
$<I / sigma(l)>$	5.76 (1.63)	18.0 (3.6)	9.0 (4.9)	9.7 (8.3)
Completeness (%)	90.89 (85.78)	99.8 (99.8)	99.72 (99.12)	99.40 (99.69)
Multiplicity	3.6 (3.5)	18.0 (3.6)	6.2 (5.3)	3.2 (3.2)
Refinement statistics				
R_{work} / R_{free}	0.21/0.25	0.18/0.19	0.17/0.21	0.18/0.19
RMSD bond lengths (Å)	0.014	0.007	0.009	0.007
RMSD bond angles (°)	1.92	1.32	0.97	0.92
Average B factor	18.72	18.59	11.51	11.89
Main chain B factor	17.26	18.14	10.44	12.04
Ligands B factor	15.10	13.10	10.23	5.14
Water molecules B factor	26.45	25.53	21.96	8.67
No. of non-hydrogen atoms				
Number of protein atoms	12542	3089	3056	6262
Number of ligands atoms	149	44	85	84
Number of water molecules atoms	1392	227	230	96
Ramachandran plot (%)				
Most favoured	95.95	96.04	95.49	95.72
Generously allowed	4.05	3.96	4.51	4.28
Outliers	0.00	0.00	0.00	0.00

Table S3. Influence on protein melting point Tm °C (as measured by Thermofluor assay) of type and concentration of a) different buffers; b) buffer salts (50 mM Tris-HCl buffer pH 8.0 supplemented with increasing concentrations of salts); c) additives (50 mM Tris-HCl buffer pH 8.0 supplemented with increasing % of cryoprotectants) and d) co-solvents (50 mM Tris-HCl buffer pH 8.0 supplemented with increasing vol% of organic co-solvent on *Ct*OYE and *Gs*OYE. All measurements have been performed in triplicate.

Additives		Concentration	*Ct*OYE	*Gs*OYE
a buffers	50 mM Tris-HCl pH 8.0		53 ± 0.25	67 ± 0.01
	100 mM KH$_2$PO$_4$ pH 7.0		53 ± 0.24	64 ± 0.08
	50 mM Na-citrate pH 6.5		53 ± 0.00	64.5 ± 0.03
b salts (mM)	(NH$_4$)$_2$SO$_4$	100	50 ± 0.00	56 ± 0.09
		200	51 ± 0.24	58 ± 0.04
		500	51 ± 0.50	61 ± 0.31
	NaCl	100	52 ± 0.24	65 ± 0.02
		200	52 ± 0.25	66 ± 0.18
		500	53 ± 0.00	66 ± 0.00
c cryoprotectants (% weight/vol)	Sucrose	10	54 ± 0.02	67.5 ± 0.13
		20	53 ± 0.05	69 ± 0.07
		30	57 ± 0.10	71 ± 0.11
		40	59 ± 0.01	72 ± 0.17
	Sorbitol	10	55 ± 0.24	68 ± 0.09
		20	57 ± 0.26	70 ± 0.06
		30	59 ± 0.00	72 ± 0.12
		40	62 ± 0.05	74 ± 0.04
	Glycerol	10	54 ± 0.25	67 ± 0.01
		20	55 ± 0.00	68 ± 0.00
		30	56 ± 0.06	69 ± 0.10
		40	56.5 ± 0.13	69 ± 0.00
d co-solvents (% vol/vol)	Ethanol	5	51.5 ± 0.05	66 ± 0.18
		10	49.5 ± 0.05	64 ± 0.18
		20	45.5 ± 0.18	61 ± 0.12
	Acetone	5	53 ± 0.00	67 ± 0.04
		10	53 ± 0.40	67 ± 0.00
		20	53 ± 0.06	67 ± 0.23
	Acetonitrile	5	53 ± 1.39	66.5 ± 0.02
		10	53 ± 0.25	66 ± 0.34
		20	51 ± 0.29	64 ± 0.20
	DMSO	5	53 ± 0.24	67 ± 0.06
		10	52 ± 0.09	66.5 ± 0.11
		20	52 ± 0.56	66 ± 0.15
		30	-	64 ± 0.05
	Dioxane	5	49.5 ± 0.48	62 ± 0.22
		10	46.5 ± 0.13	59 ± 0.33
		20	42 ± 0.21	55 ± 0.02

Table S4. Preliminary spectrophotometric screening of *Ct*OYE and *Gs*OYE.

Substrate	U/mg	
	***Ct*OYE**	***Gs*OYE**
O₂	0.70 ± 0.15	0.98 ± 0.17
1a	2.0 ± 0.04	2.3 ± 0.26
4a	4.8 ± 2.67	4.1 ± 0.26
5a	3.4 ± 0.25	1.7 ± 0.00
7a	3.4 ± 0.10	N.D.
18a	17.5 ± 0.65	7.1 ± 0.09
19a	6.4 ± 0.30	2.4 ± 0.09
20a	6.9 ± 1.72	4.4 ± 0.78
21a	12.3 ± 0.40	1.7 ± 0.35

The standard assay (100 μL) was performed at 25 °C in 50 mM Tris-HCl, 150 mM NaCl (pH 8.0) containing 100 μM NADPH and 10 mM of substrate. The reaction was started through the addition of enzyme to a final concentration of 200 nM. N.D. not detected. All measurements have been performed in triplicate. Background NADPH oxidase activity was measured in the absence of alkenes (first row, molecular oxygen present in the air as substrate) but it was not subtracted from the specific activity with the other substrates.

Table S5. Bioreduction of selected substrates at 50-100 mM concentration[a]

Substrate	*Ct*OYE Conv.(%)	*Gs*OYE Conv. (%)
1a	52	54[#]
2a	8	1.3[#]
4a	76 (34[#b])	96 (25[#b])
5a	42	53
7a	60	52
8a	11	2
11a	46	54

[a]The standard assay (500 μL) was performed at 30 °C and 120 rpm in 50 mM Tris-HCl (pH 8.0) containing 1 mM NAD^+, 10 U/mL GDH, 100 mM glucose and 50 mM of substrate. The reaction was started through the addition of enzyme to a final concentration of 100 μg/mL and incubated overnight. The conversion reported is based on product formation or substrate consumption (**11a**) according to calibration curve with authentic reference material. All measurements have been performed in duplicate. The data points are mean values of duplicate reactions. Deviation from mean values was below 5% or below 10% where indicated ([#]).

[b]Standard conditions except 100 U/mL GDH, 200 mM glucose, 100 mM substrate and 200 μg/mL enzyme.

[c]The conversions for **4a** are reported as apparent conversion (area product/(area product + area substrate)*100).

Table S6. Influence of temperature and reaction time on the enantiopurity of **17b** formed through biocatalysed reduction of 10 mM **17a** by *Ct*OYE and *Gs*OYE[a]

	*Ct*OYE	*Gs*OYE	
pH	10 °C / 6 h	10 °C / 6 h	25 °C / ON
5	70 (R)	50 (R)	*rac*
6	68 (R)	43 (R)	*rac*
7	32 (R)	22 (R)	*rac*
8	*rac*	*rac*	*rac*

[a]Reaction conditions (500 µL): 50 mM Tris-HCl (pH 5.0 - pH 8.0) containing 500 µM NAD_+, 10 U/mL GDH, 50 mM glucose and 10 mM of substrate. The reaction was started through the addition of enzyme to a final concentration of 100 µg/mL and incubated overnight at 25 °C or 10 °C, 120 rpm overnight or 6h. All measurements have been performed in duplicate. The data points are mean values of duplicate reactions. Deviation from mean values was below 5%.